SODANKYLÄ GEOPHYSICAL OBSERVATORY
PUBLICATIONS

OULUN YLIOPISTO
UNIVERSITY of OULU

No. 111

3D STRUCTURE OF THE CRUST AND UPPER MANTLE BELOW NORTHERN PART OF THE FENNOSCANDIAN SHIELD

HANNA SILVENNOINEN

Sodankylä 2015

SODANKYLÄ GEOPHYSICAL OBSERVATORY PUBLICATIONS

OULUN YLIOPISTO
UNIVERSITY of OULU

No. 111

3D STRUCTURE OF THE CRUST AND UPPER MANTLE BENEATH NORTHERN FENNOSCANDIAN SHIELD

HANNA SILVENNOINEN

Academic dissertation
University of Oulu Graduate School
Oulu Mining School

Academic dissertation to be presented with the assent of the Doctoral Training Committee of Technology and Natural Sciences of the University of Oulu, in GO101 lecture hall of the University of Oulu on 18th December 2015 at 11 o'clock.

Sodankylä 2015

SODANKYLÄ GEOPHYSICAL OBSERVATORY PUBLICATIONS
Editor: Dr Thomas Ulich
Sodankylä Geophysical Observatory
FI-99600 SODANKYLÄ, Finland

This publication is the continuation of the former series
"Veröffentlichungen des geophysikalischen Observatoriums
der Finnischen Akademie der Wissenschaften"

Sodankylä Geophysical Observatory Publications

ISBN 978-952-62-1067-4 (paperback)
ISBN 978-952-62-1068-1 (pdf)
ISSN 1456-3673

OULU UNIVERSITY PRESS
Sodankylä 2015

Abstract

The crustal and upper mantle structures of the Shield on the regional scale were investigated using the data of the POLENET/LAPNET passive seismic array and the previously published models of active and passive seismic experiments in the study area. This area is centred in northern Finland and it extends to surrounding areas in Sweden, Norway and northwestern Russia. The bedrock there is mostly of the Archaean origin and the lithosphere of the region was reworked by two orogenies during Palaeoproterozoic.

One of the results of the thesis was a new map of the Moho depth of the study area, for which new estimates of the crustal thickness were obtained using receiver function method and complemented by published results of receiver function studies and controlled source seismic profiles. The map differs from the previously published maps in two locations, where we found significant deepening of the Moho. The 3D structure of the upper mantle was studied using teleseismic traveltime tomography method. The resulting model shows high seismic velocities below three cratonic units of the study area, which may correspond to non-reworked fragments of cratonic lithosphere and a low velocity anomaly separating these cratonic units from each other.

The regional scale studies were complemented by two smaller scale studies in upper crust level using combined interpretation of seismic profiling and gravity data. These studies were centred on Archaean Kuhmo Greenstone Belt in eastern Finland and central Lapland in northern Finland located in the crust reworked during Palaeoproterozoic. Both areas are considered as prospective ones for mineral exploration. Both studies demonstrate the advantage of gravity data inversion in studying 3D density structure of geologically interesting formations, when the Bouguer anomaly data is combined with *a priori* information from petrophysical and seismic datasets.

Keywords: Fennoscandia, crust, upper mantle, Bouguer anomaly, density modelling and inversion, P-wave velocity, teleseismic tomography, receiver function, controlled source seismic methods

Acknowledgments

I have deepest gratitude to my primary supervisor professor Elena Kozlovskaya for her continuous support through all these years and for introducing me to the world of seismology. She has challenged me to learn both field working and seismic data handling and supported my learning in modelling and inversion of both seismic and gravity data. I express my gratitude also to my second supervisor professor Pertti Kaikkonen especially for his support with administrative issues and other practical matters that made my work easier. I thank Sodankylä Geophysical Observatory for all the financial support I got and the possibilities to travel to various international conferences and scientific visits. I also thank the staff and PhD students of both Sodankylä Geophysical Observatory and Geophysics Department of Oulu Mining School for all good discussions and technical help. The special thanks go to Dr. Markku Pirttijärvi for his help with the modelling and inversion of Bouguer anomaly data. The Academy of Finland funded a part of my dissertation work through POLENET/LAPNET project. I thank also Vilho, Yrjö ja Kalle Väisälä foundation, Apteekin rahasto, the Faculty of Science of University of Oulu, Outokumpusäätiö, Moneta, Tauno Tönning foundation, Suomalainen Konkordia-liitto and Tekniikan edistämissäätiö for financial support during my dissertation work.

Thanks to the financial support of the Academy of Science of Check republic I was able to visit professor Jaroslava Plomerová and her staff and students in Prague. Her lessons in handling and picking teleseismic datasets have been invaluable. The financial support of Sodankylä Geophysical Observatory, ETH Zürich and Doctoral Program of Geosciences in Finland made it possible for me to visit professor Edi Kissling and his students in Zürich in multiple occasions. I gratefully acknowledge all the help I got from his lessons in 3D modelling and inversion of seismic data. The wealth of knowledge I have gained from scientific visits abroad is only widened by the good friends I have found on these trips.

Finally I would thank my love Arto, my parent and all my friends for all the patience and support during my studies. I could not have done it without you all.

Contents

Original publications

This thesis consists of an introductory part and the following original papers:

I H. Silvennoinen and E. Kozlovskaya, *3D structure and physical properties of the Kuhmo Greenstone Belt (eastern Finland): Constraints from gravity modelling and seismic data and implications for the tectonic setting*, Journal of Geodynamics, **43** (2007), 358–373.

II H. Silvennoinen, E. Kozlovskaya, J. Yliniemi and T. Tiira, *Upper Crustal Velocity and Density Models Along FIRE4 Profile, Northern Finland*, Geophysica, **46(1-2)** (2010), 21–46.

III H. Silvennoinen, E. Kozlovskaya, E. Kissling, G. Kosarev and POLENET/LAPNET Working Group, *A new Moho boundary map for the northern Fennoscandian Shield based on combined controlled-source seismic and receiver function data*, GeoResJ, **1-2** (2014), 19–32.

IV H. Silvennoinen, E. Kozlovskaya and E. Kissling, *Teleseismic P-wave traveltime tomography model of the upper mantle below northern Fennoscandia*, Solid Earth Discuss, **7** (2015), 2527–2562.

In the text, the original papers will be referred to by their Roman numerals.

The contributions of the author to the original publications are as follows:

Paper I: 3D structure and physical properties of the Kuhmo Greenstone Belt (eastern Finland): Constraints from gravity modelling and seismic data and implications for the tectonic setting

This paper introduces the results of a 3D modelling and inversion of the structure of Kuhmo Greenstone Belt. Available gravity and seismic data was used in estimating the density and seismic velocity of the belt. The author did all modelling and inversion, participated in discussions and interpretations and wrote significant portion of the text, including the descriptions of the study area, data, methodology and results.

Paper II: Upper Crustal Velocity and Density Models Along FIRE4 Profile, Northern Finland

The main results of this paper are 2D seismic models based on forward modelling and inversion of wide-angle reflection and refraction data recorded along FIRE4 profile in central Finnish Lapland and 3D density models of the region using both forward modelling and inversion of Bouguer anomaly data. The author participated in pre-processing and picking of the seismic data, did all the modelling, participated in the discussion and the interpretation of the results and wrote most of the text.

Paper III: A new Moho boundary map for the northern Fennoscandian Shield based on combined controlled-source seismic and receiver function data

This paper introduces a new Moho map of northern Finland and surrounding areas. The map is based on previous controlled source seismic and receiver function results complemented by new receiver function results based on POLENET/LAPNET data presented in this paper. The author participated in the field campaign and the data processing of POLENET/LAPNET array, did the picking of the teleseismic data as well as the calculations of the receiver functions and the inversion to S-wave velocity models using the inversion code edited for this paper by Grigoriy Kosarev. The author did the evaluation and error estimation of the existing controlled source seismic models, participated significantly in discussion of the obtained Moho depth map and wrote most of the text.

Paper IV: Teleseismic P-wave traveltime tomography model of the upper mantle below northern Fennoscandia

This paper presents the results of teleseismic P-wave traveltime tomography based on the data of POLENET/LAPNET array as well as those parts of the SVEKALAPKO array that overlap with POLENET/LAPNET study area. The author did the picking of the teleseismic P-wave data as well as the inversion, participated significantly in the discussion and conclusions of the results and wrote most of the text.

Chapter 1

Introduction

1.1 Background and research environment

Northern Fennoscandian Shield has lately been under heavy interest from mining community. In 2014 Fraser Institute Annual Survey of Mining Companies placed Finland on 1st position in investment attractiveness and Sweden as 12th worldwide (1st and 3rd in Europe) [33]. The survey assesses both geological attractiveness and public policy factors such as attitudes towards mining, taxation and political stability of the area. Geologically the Precambrian shield covering most of Fennoscandia is similar to the mineral-rich areas around the world (e.g. Australia, South Africa and Canada). The region has long tradition in mining as well as a large number of active mines. Despite the long and active mining history, the region has great potential for significant future discoveries as many parts of Fennoscandia are under-explored [18, 19].

In ore geology the process of locating ore potential areas starts from large-scale studies and proceed to smaller scale. According to Pohl [73] there are three major target sizes in the process:

1. Ore province scale, which concentrates on the regional scale mapping of mineral deposits of similar origin from deeper crust or mantle, where the ores of the region were derived from.

2. Ore belt or ore district scale, which concentrates on studying a single block of the crust with deposits of genetically close ores. The belts and districts are generally associated with tectonic structures inside an ore province.

3. Mineral or ore deposit scale, which concentrates on mapping natural concentrations of useful minerals in quantities that can be economically exploited.

Geophysics has a part in all three phases of prospecting. In regional scale, geophysics can be used to estimate the 3D position of major tectonic units, metamorphic complexes and major suture zones. The required information includes also details of

crustal thickness and estimates of crustal and mantle composition to estimate from where the ores were originally drawn. The seismic methods can give reliable information at lower crustal and upper mantle depths required for ore province scale mapping. The seismic methods are complemented in the depth range by magnetotelluric (MT) method studying the electrical conductivity structure at the lithospheric depths by measuring Earth's electromagnetic field. See [14] for a recent PhD study using MT method in Fennoscandian Shield.

As the number of geophysical, especially seismic, studies in northern Finland is smaller than the number of studies in southern Finland (e.g. [35]), the crustal models of the area were based on limited amount of data only and previous seismic mantle models were virtually non-existent. When within the umbrella of International Polar Year 2007 – 2009 a passive seismic array measurement POLENET/LAPNET recorded a significant amount of new seismic data spread over the whole northern Finland and surrounding areas in Sweden, Norway and Russia, one of the main goals of the project was to improve the regional geophysical models of the crust and upper mantle.

The ore belt scale is still too large to be easily drilled for direct information of the rock types and the presence of ores. The indirect methods of geophysics are needed to give the most reliable estimates of the structures and materials below the surface layer. While in ore deposit scale the results of geophysical studies are generally qualified by drilling, the geophysical methods can help to analyse the continuations of the structures between drill sites and to point drilling to most interesting and important sites. In these scales the multitude of geophysical methods are available and the choice should be based on the *a priori* information and assumptions on the properties of the study area.

In the ore belt scale studies included in this thesis, we concentrated on gravity based methods as the Bouguer anomaly data set in regular grid is available for whole Finland making it possible to reliably compare the results obtained from different study regions. The gravity based methods were complemented by seismic methods and the previously published models of the high quality crustal scale seismic profiles, particularly near-vertical reflection seismic profiles of the FIRE project [51], crossing the selected study areas.

1.2 Study area: Northern Fennoscandian Shield

The study area of this thesis is located in the northern part of the Fennoscandian Shield (sometimes also called Baltic Shield). Geographically Fennoscandian Shield covers from west to east Sweden, Finland, and northwestern parts of Russia. This study is centred in northern Finland and it extends to surrounding areas in Sweden, Norway and Russia (see Figure 1.1).

Fennoscandian Shield forms the northern part of the East European Craton, which is separated by the Trans-European Suture Zone from the Phanerozoic part of Europe [25]. The Shield consists of its Archaean nucleus and Proterozoic terranes accreted along its southern and western flanks. In the study area of this thesis, the main tectonic components are the three Archean cratonic units: Karelian Province forming

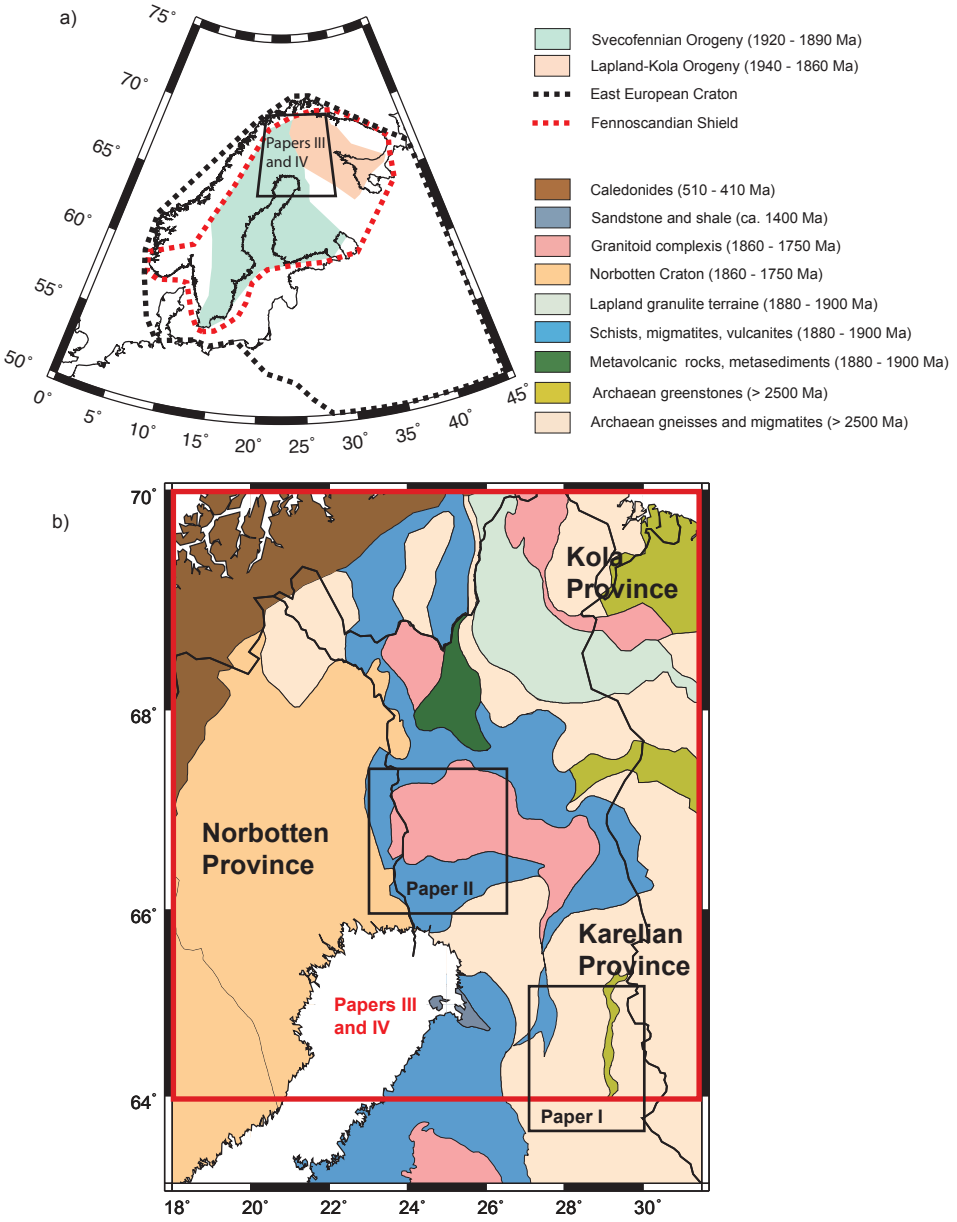

Figure 1.1: A map of northern Fennoscandian Shield and the study areas of the Papers I - IV. Subplot a) shows the location of the East European Craton and Fennoscandian Shield [25] as well as the two main orogenies in our study area [52]. Subplot b) shows a simplified geological map of the area based originally on 1:2000000 geological map of Fennoscandia [43]. The three cratonic provinces forming the area are indicated on the map. The study areas of the Original Papers of this thesis are marked on the maps as well.

most of the study area, Kola Province in northeast and Norrbotten Province in western part of the study area (see Figure 1.1b).

According to Gaál and Gorbachev [24] the Post-Archaean development of the Archaean crust of Fennoscandia started by rifting events that created the three main tectonic units covering the study area. Rifting began in northeast and led to separation of cratonic components by oceans around 2.1 Ga [16, 24]. The rifting event was followed by subduction of the new oceanic crust and subsequent island arc accretion in 1.95 – 1.91 Ga and two orogenies: the Lapland-Kola orogeny (1.94 – 1.86 Ga, [16]) and the northern part of the composite Svecofennian orogeny (1.92 – 1.89 Ga, [52]). The location of the orogenies inside the study area are shown in Figure 1.1b). Although in general Svecofennian orogeny formed large units of new crust, both its northern part and Lapland-Kola orogeny comprise mainly of reworked Archaean crust with only a minimal amount of juvenile material [52].

Most of the economic mineral deposits in Fennoscandia are located in Proterozoic part of the crust and were formed during the period of the short-lived but intense orogenies [90]. After these two orogenies the area has been relatively stable, although there was some small volume magmatism with ages ranging from Palaeoproterozoic to Devonian especially in eastern part of the study area [17]. These younger formations are chemically quite diverse but generally share a relatively deep source from mantle depths [92].

1.3 Overview of previous seismic studies in the region

The lithospheric structure of the Fennoscandian Shield has been studied by several controlled source seismic (CSS) projects in different parts of the shield ([9, 26, 29, 35, 51, 56, 10], Figure 1.2). Most of these projects were aimed to investigate the structure of the crust but most prominently FENNOLORA [29] crossing the whole Sweden from south to north allows investigation of the upper mantle structures, too.

There are six major CSS profiles within the study areas of this thesis. Of the transects of near-vertical reflection seismic FIRE project [51], FIRE4 crosses the central part of the study area and the northern part of FIRE1 touches the southernmost part. The wide-angle reflection and refraction profiles crossing the study area are FENNOLORA [29] in Sweden, POLAR [35, 56] and SVEKA'81 [58, 50] in Finland and PECHENGA-KOSTOMUKSHA [9] in Russia. All the profiles are roughly north-south directed and FIRE4 and POLAR are almost co-located in the northern part of FIRE4 transect (FIRE4A profile). In addition to these six profiles HUKKA07 [84] is a recent wide-angle reflection and refraction profile using commercial and military chemical explosion sites as sources of seismic signal. The rest of the CSS profiles in northern Finland are mostly one or two shot point wide-angle reflection and refraction profiles giving mostly 1D information of the crust.

In addition to controlled source seismic profiles, parts of Fennoscandian shield have been covered by passive seismic array measurements. The two largest arrays are TOR [78] in southern Sweden and SVEKALAPKO [31, 75] in southern and central Finland. The projects increased significantly our understanding of the structure and

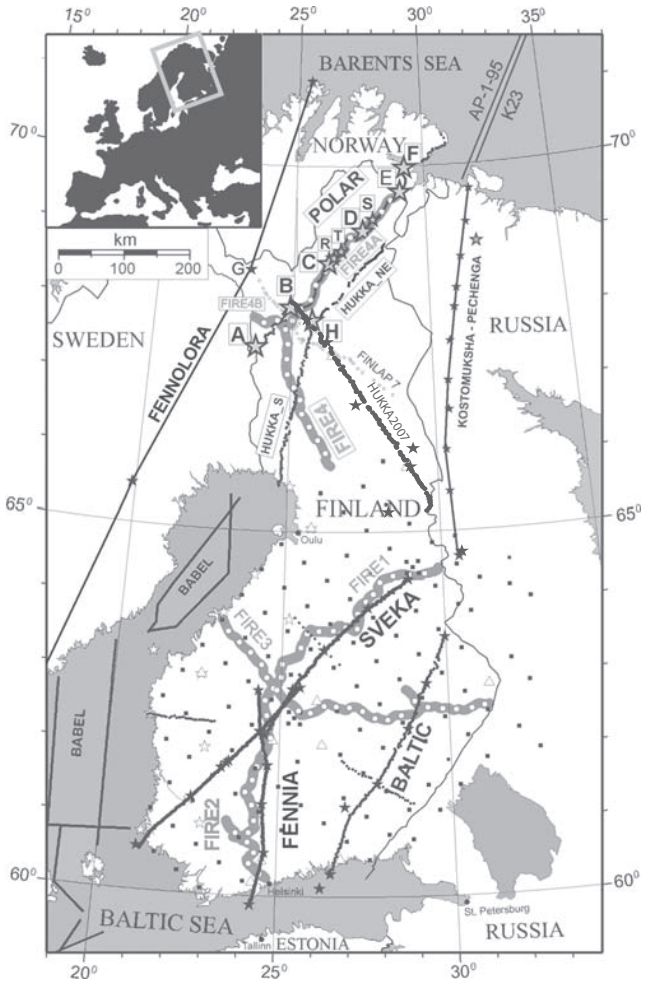

Figure 1.2: A map of CSS profiles prior to POLENET/LAPNET project and the seismic stations of SVEKALAPKO array. The figure is modified from Janik et al. [35] by adding HUKKA2007 to it. The CSS profile locations are shown in black with shot-points marked by stars. FIRE transects are marked with grey with white dots. The black dots mark the locations of SVEKALAPKO seismic stations.

evolution of Fennoscandian shield. The SVEKALAPKO array can be considered the predecessor of POLENET/LAPNET and it was was operational 1998 – 1999. SVEKALAPKO study area overlaps slightly with POLENET/LAPNET to make the comparison of results produced by the projects easier, and together the two arrays cover whole Finland and to some extend the surrounding areas. The SVEKALAPKO array consisted of 55 broadband and 88 short period instruments and it was deployed with the aim of resolving the local lithospheric structures.

The teleseismic P-wave tomography results of SVEKALAPKO study area [75] revealed a deep high velocity cratonic root below the central Finland. On the other hand, the main tectonic feature, the boundary between Archaean and Proterozoic terranes that was clearly seen in surface wave analysis and anisotropy studies [12, 71], was not visible in tomography results. The information on the crustal structure of southern and central Finland based on SVEKALAPKO data was complemented by local earthquake tomography [32] and receiver function [4, 49] studies.

An additional relatively dense array of seismometers in Fennoscandia is formed by the permanent station array SNSN in Sweden. As the northern stations of SNSN form the western part of POLENET/LAPNET array, the studies done with SNSN data usually overlap with POLENET/LAPNET study area. Similarly to other seismometer arrays, SNSN data has been used in multitude of seismic studies in crustal and upper mantle scale (e.g. [20, 62]).

1.4 Passive seismic POLENET/LAPNET array

POLENET, the Polar Earth Observing Network (http://www.polenet.org), was one of the key geophysical projects of the latest International Polar Year 2007 – 2009. It was a multidisciplinary experiment aiming to improve the geophysical observations across the Polar Regions. Existing and new seismic stations and Global Positioning Systems (GPS) constituted the main part of the deployments carried out as parts of POLENET but also magnetic, gravity, tide-gauge and other types of geodetic observations were included.

POLENET/LAPNET was a sub-project of POLENET. The POLENET/LAPNET array (see Figure 1.3), located in northern Fennoscandia between 64° – 70° N and 18° – 32° E, consisted of 37 temporary and 21 permanent seismic stations. All of the station sites except for 2 temporary stations had broadband sensors deployed at least for a part of the data acquisition period. The array registered waveforms from teleseismic, regional and local earthquakes and other seismic events from May 2007 to September 2009. The main target of the POLENET/LAPNET array, in addition to monitoring glacial earthquakes of Greenland, was to increase our knowledge of the structures of the crust and upper mantle of northern Fennoscandia and, if possible, to find the depth of the lithosphere-asthenosphere boundary (LAB).

POLENET/LAPNET project was a major part of my PhD thesis work. I was in some capacity participating in almost every practical aspect of fieldwork from participating in negotiations with station site owners to the deployment, service and uninstallation of the temporary stations throughout the data acquisition period. The temporary part

of the array consisted of 6 different brands or sub-brands of sensors and 6 different brands of data loggers, each with slightly different features, software and service requirements, giving a good overview of the instrumentation available in passive seismic field of the day. In addition to fieldwork, I took part in pre-processing and compiling the data and metadata from different data logging systems and raw data formats to fit into POLENET/LAPNET data centre requirements, participated in data quality control and finally actually used the data in Papers III and IV of this thesis.

During the data processing, quality control and analysis, the experience from fieldwork and with these particular stations turned out to be highly valuable. It was relatively easy to speculate on peculiarities in the data from different stations and different parts of data acquisition period, as I was familiar with the details of the installation plan as well as any changes in equipment, installation and the infrastructure and in nature, weather and other details surrounding the stations.

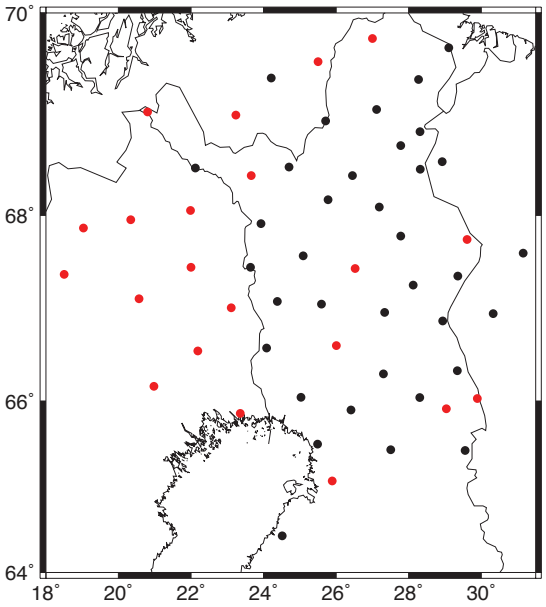

Figure 1.3: The station map of POLENET/LAPNET array. Permanent seismic broadband station are marked with red dots and temporary seismic stations with black dots.

1.5 Objectives and scope of this thesis

This thesis is based on two research papers studying the lithospheric structures in regional scale and two papers studying the upper part of the crust in local (ore belt) scale. Paper III presents an updated Moho depth map of POLENET/LAPNET study area of roughly 700 km x 700 km. The map is based on previously published and new seismic studies. Paper IV presents the upper mantle structure also

in POLENET/LAPNET study area using teleseismic P-wave traveltime tomography method. In local scale Paper I concentrates on the 3D structure of Kuhmo Greenstone Belt in eastern Finland and Paper II presents modelling and inversion results in northern Finland in Central Lapland Granitoid Complex area. Both Papers I and II use Bouguer anomaly data as the main dataset complimented with available seismic data.

The main objectives of the current study are

- To obtain an updated 3D model of the crust below POLENET/LAPNET study area;
- To obtain a 3D model of seismic velocity perturbation in upper mantle below POLENET/LAPNET study area and find lithosphere asthenosphere-boundary, if possible;
- To evaluate the 3D structure of the Archaean Kuhmo Greenstone Belt and its implications on the evolution of the Belt;
- To evaluate the 3D structure of Central Lapland area with special interest in the source of the positive anomaly inside Central Lapland Granitoid Belt and the ore potential Peräpohja Schist Belt and Kittilä Greenstone Belt.

In following chapters I summarize the main details of the gravity and seismic data and the modelling and inversion methods used, summarize the results of the Papers I – IV and discuss briefly the implications of the results.

Chapter 2

Gravity modelling and inversion

2.1 Basic theory and the data

The gravitational attraction of Earth's mass, the elliptical shape of the Earth and its rotation around its axis cause most of the gravity field measured at or close to Earth's surface. In addition to surface topography, tidal effects of the Sun and Moon, and the effects caused by movement and elevation of the measurement platform, the density variations inside the Earth form slight anomalous variations to this field. The initial step in gravity analysis is to properly separate the field caused by the study volume from the field of the surrounding universe. As a consequence there are several ways to represent the measured gravity field. The most common ones in geological applications are Bouguer anomaly maps and their derivatives, as they display well the density variations of soil and bedrock [21].

In the most basic level of gravity theory, the gravitational attraction between two masses was defined by Isaac Newton in 1687: the magnitude of the gravitational force F between two masses is proportional to each mass and inversely proportional to the square of their separation

$$F = \gamma \frac{m m_0}{d^2}, \tag{2.1}$$

where γ is Newton's gravitational constant, m and m_0 are the two masses and d is the distance between their centres of mass.

The gravitational potential, or Newtonian potential, is the work done by a gravitational force on an unit mass if the unit mass is moved from its current location to a predefined reference location. In general form the gravitational potential of the mass m at the distance of d from its centre of mass is

$$U = \gamma \frac{m}{d} = \gamma \frac{m}{\mid \mathbf{r_i} - \mathbf{r} \mid}, \tag{2.2}$$

where $\mathbf{r}$ and $\mathbf{r_i}$ are the Cartesian coordinates of the mass producing the gravitational field and the unit mass, respectively, and the gravitational attraction $\mathbf{g}$ caused be the

mass m and affecting the unit mass at location $\mathbf{r_i}$ is

$$\mathbf{g}(\mathbf{r_i}) = \bigtriangledown U = -\gamma \frac{m(\mathbf{r_i} - \mathbf{r})}{\mid \mathbf{r_i} - \mathbf{r} \mid^3}, \tag{2.3}$$

In geophysical gravity based methods the commonly measured quantity is the vertical component of the attraction g_z. At location $\mathbf{r_i}$ it can be defined as

$$g_z(\mathbf{r_i}) = -\gamma \frac{m(z_i - z)}{\mid \mathbf{r_i} - \mathbf{r} \mid^3} = -\gamma \int_V \rho(\mathbf{r}) \frac{z_i - z}{\mid \mathbf{r_i} - \mathbf{r} \mid^3} dv, \tag{2.4}$$

where V is the volume of the object causing the gravity field and $\rho(\mathbf{r})$ is the mass distribution inside V.

The gravity measurement net by the Finnish Geodetic Institute forms the basis of the gravity datasets in Finland. The net covers whole country with average station spacing of 5 km [37]. The Geological Survey of Finland has used this data to compile and publish different gravity based maps, including the Bouguer anomaly map and its derivatives [21]. In Papers I and II, a digital 1:2000000 Bouguer anomaly map of Finland compiled as a part of the Bouguer anomaly map of Fennoscandia was used [45].

The complete Bouguer anomaly Δg_{cb} can be written as

$$\Delta g_{cb} = g_{obs} - g_{fa} - g_{sb} - g_t - g_0, \tag{2.5}$$

where g_{obs} is the observed gravity and g_0 is the theoretical gravity which takes into account the mass, shape and rotation of the Earth. The correction g_{fa} corrects for the distance of the measurement from the sea level, but not for the gravity effects caused by the material (bedrock and soil) between sea level and the measurement point (so called free air correction). The simple Bouguer correction g_{sb} corrects for this effect by assuming an infinite slab with normal crustal density of 2670 kg/m^3 between sea level and measurement point. Especially in areas with strong topographic variations also a terrain correction g_t is needed, as it adjusts for the effect of the masses above (when measuring in low elevation) or the missing masses below (when measuring in higher elevation) the measurement point. [11]

After all the corrections, the obtained Bouguer anomaly data contains anomalies caused by density variations inside the Earth. As the interest of the modelling is inside the selected study volume, the anomalous masses outside the study volume must be compensated by introducing a regional gravity field. The regional field can be estimated from the Bouguer anomaly data or it can be derived from other sources. While estimating the field from the data, the most common method is to use upward continuation, which transforms the data from one level to another. This process attenuates the anomalies caused by the close-by sources more than the anomalies caused by the ones further away.

In Papers I and II we used a previous 3D density model of southern and central Finland by Kozlovskaya et al. [48] to calculate the regional field. The model is

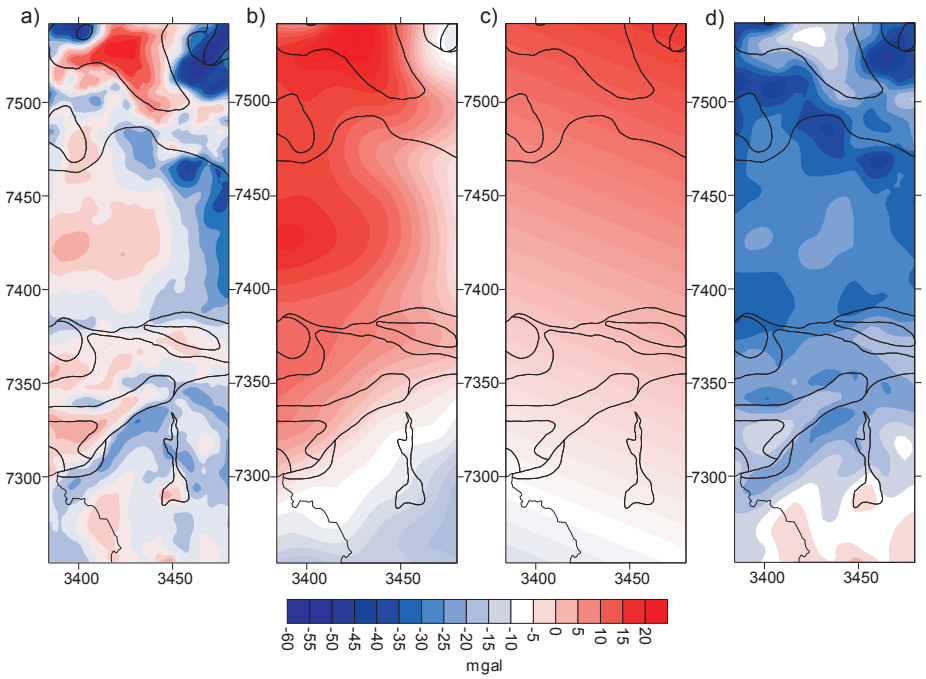

Figure 2.1: The subplot a) shows the Bouguer anomaly in the study area of paper II, the subplot b) shows the regional anomaly calculated from Kozlovskaya et al. [48], the subplot c) shows the base anomaly calculated with Grablox software, and the subplot d) shows the residual anomaly after regional and base anomalies are excluded from Bouguer anomaly.

based on previous seismic studies and the results of petrophysical studies of bedrock density in Finland and was finalized using Bouguer anomaly inversion. The model extends from surface to the depth of 70 km and describes the crust by dividing it to major crustal units only. In addition to regional anomalous field, also a linear so-called base anomaly was used in both papers. The base anomaly takes care of even deeper anomalous trends in the data as well as possible levelling inconsistences between Bouguer anomaly and regional field data. See Figure 2.1 for the original Bouguer anomaly data used in Paper II, the regional anomaly field calculated from Kozlovskaya et al. [48], the base anomaly and the residual Bouguer anomaly after removing regional and base anomalies.

Most of the geophysical data, most notably potential field data (gravity and magnetic data) are non-unique in the sense that there are an infinite number of models, which explain the data within its error bars. The more additional data can be used, be it geophysical, geological or some other type, the more the non-uniqueness is decreased [30]. In Papers I and II seismic and petrophysical data was used in addition to geological maps for this purpose. Additionally both forward modelling and different

types of inversion and inversion parameters were tested to obtain slightly different results for additional uncertainty estimation.

2.2 Forward modelling and inversion of Bouguer anomaly data

Software called Grablox by Pirttijärvi [69] was used for 3D gravity modelling and inversion in Papers I and II. In Grablox the density model is parameterized as a 3D orthogonal block model with constant density value within each cell. The horizontal dimensions of the cells are fixed and either cell densities or vertical dimensions or both can be optimized [69].

In forward modelling the initial model is constructed based on *a priori* information or assumptions on density structures within the target volume. The anomalous gravity field caused by the model is calculated and compared to observed anomaly. If required fit is not found, the model is adjusted and a new theoretical gravity field is calculated. In the block model Grablox uses, the Equation (2.4) can be reformulated as a sum

$$g_{z,m} = \sum_{n=1}^{N} (\gamma V_n \frac{z_n - z_m}{\mid \mathbf{r_n} - \mathbf{r_m} \mid^3}) \rho_n = \sum_{n=1}^{N} G_{mn} \rho_n, \tag{2.6}$$

where $\mathbf{r_n}$ is the location of the nth block centre and $\mathbf{r_m}$ is the location of the observation point m and z refers to the depth of each point (positive axis points down). Or in matrix format

$$\mathbf{g_z} = \mathbf{G}\rho \tag{2.7}$$

where $\mathbf{g_z}$ is a vector of M observations, ρ is a vector of N blocks in the model and $\mathbf{G}$ is a (MxN) matrix of G_{mn}.

In addition to forward calculation of the gravity field caused by the study volume, Grablox can do inversion using two inversion schemes: linearized inversion based on singular value decomposition (SVD) with an adaptive damping method described by Pirttijärvi [68] and Occam inversion. The inversion aims to adjust the model parameters so that the dataset calculated from the model fits with the observed dataset at desired level.

In linearized, SVD based inversion the equation to estimate the model parameter vector $\mathbf{m_{est}}$ is

$$\mathbf{m_{est}} = (\mathbf{G^T W_d G} + \varepsilon \mathbf{W_m})^{-1} \mathbf{G^T W_d g_z}, \tag{2.8}$$

where $\mathbf{W_d}$ is data weighting matrix, $\mathbf{W_m}$ is model smoothing matrix and ε^2 is damping value used [60].

The alternative to SVD based inversion in Grablox is Occam's inversion. The method utilizes so called Occam's razor principle, which emphasizes the importance of finding the simplest possible model to explain the data. Occam's inversion was introduced by Constable et al. [15] for electromagnetic data. In it the roughness of the model (difference between a block and the average density of the blocks surrounding it) is optimized together with the fit between measured and computed data. A resulting

model may not fit the data as well as a model obtained by SVD based inversion as it is smoothed by using the neighbouring parameter values as inversion constraints [15, 69]. The results of SVD based and Occam's inversion were compared in Paper I. However, the advantage of the Occam's inversion is that if there is some fixed *a priori* data available in the initial model, the method will constrain the parameter values of the surrounding blocks close to that data. This feature was utilized in Paper II where 3D gravity inversion was done based on the *a priori* information of surface densities from petrophysical data.

Chapter 3

Crustal scale seismic methods

Seismic methods are a widely spread group of geophysical methods, in which mechanical vibrations, seismic waves, are used to study the structure of the Earth. The source of the waves can be manmade, for example explosion, or it can be natural, most commonly a tectonic earthquake. The methods using manmade source are often called active or controlled source seismology (CSS), as the wave generation requires an active participation of the scientist making the source parameters like location, onset time and signal strength easy to control. Consequently the methods studying the inner structure of the Earth using natural sources are often called passive seismic methods. Despite the differences in signal generation, the laws governing the behaviour of the seismic waves travelling through the Earth stay the same.

All the seismic methods used in this thesis rely on seismic ray theory. The propagation of seismic wave front is simplified as a single ray, a seismic ray, pointing in the direction of the energy flow from the source to the receiver through the study media. The main assumption of the theory is that the frequency of the wave is infinitely high or at least high enough to be significantly higher than the topographical features of the seismic interfaces inside the Earth [77]. The basis of most of the ray theory is the eikonal equation

$$(\bigtriangledown T)^2 = (\partial_x T)^2 + (\partial_y T)^2 + (\partial_z T)^2 = \frac{1}{c^2}, \tag{3.1}$$

where T is called the traveltime function and c is the wave velocity. The gradient of the traveltime function can be used to define the local wave velocity and ray direction:

$$\bigtriangledown T = \mathbf{s}, \tag{3.2}$$

where the vector $\mathbf{s}$ is the local slowness vector and its direction is the ray direction and the inverse of the length is the local wave velocity [77].

The seismic ray theory is most often used to calculate the traveltime, the time it takes for the seismic wave to reach the receiver, for a seismic wave. According to Fermat's principle, the ray path between two points is that for which the traveltime is at minimum. In homogenous media the ray path is a straight line. In heterogeneous media the ray will alter direction to find the fastest and generally more complex route.

In general form the traveltime is the sum of the traveltimes through each portion of the ray path

$$t = \int_S \frac{ds}{c} \tag{3.3}$$

where t is the total traveltime, c is the seismic velocity field the ray passes through and S is the ray path.

As not only traveltime but also the ray path depends on the velocity field, the path has to be known before the theoretical traveltime through the velocity field can be calculated. At a seismic velocity interface the seismic wave changes direction according to Snell's law [3]

$$\frac{sin(i_1)}{\alpha_1} = \frac{sin(i_2)}{\alpha_2} = \frac{sin(j_1)}{\beta_1} = \frac{sin(j_2)}{\beta_2} = p, \tag{3.4}$$

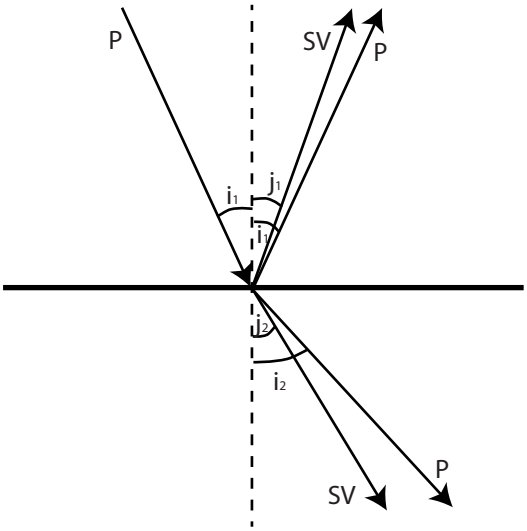

Figure 3.1: P-wave at a seismic interface and the resulting four derivative rays: refracted and reflected P wave and refracted and reflected S waves. The enumerations and symbols equal to those used in Equation (3.4)

where α_1 and α_2 are the P-wave velocities in layers 1 and 2, respectively, β_1 and β_2 the S-wave velocities in both sides of the boundary, i_1, i_2, j_1 and j_2 are the corresponding incidence angles, and p is the ray parameter, which stays constant for a seismic wave. Figure 3.1 presents a sketch of the rays formed at seismic interface. In general all four types of waves are generated, though the respective amplitudes vary significantly on the incidence angle i_1 [2]. When the incidence angle is relatively small, most of the energy of the wave crosses the boundary, and when the incidence angle is relatively large, most of the energy is reflected back. Additionally, the higher the velocity in lower layer 2, the higher percentage of the seismic energy is reflected back. The effect of gradual change in seismic velocity on the path of a seismic ray can either be

approximated to desired accuracy by layers of constant velocity and applying Snell's law at all cell boundaries or by solving Equation (3.3) inside the layer.

3.1 Controlled source seismic methods

In controlled source seismic (CSS) method, as the name suggest the source is man-made, traditionally explosives. The CSS methods can be divided to two main groups: near-vertical reflection method and wide-angle reflection and refraction method. The main difference in data acquisition is the distance of the receivers from the source. In near-vertical reflection studies (Figure 3.2a) the receivers are located relatively close to the source, in crustal scale studies within some kilometres, and the data can be used to obtain detailed images of subsurface layers and other seismically reflective structures. The method has a long history with oil industry, as it is particularly sensitive to strong horizontal velocity contrasts common in oil traps. In wide-angle reflection and refraction studies receivers are further, up to hundreds of kilometres, away and the main interest is on refracted waves with reflected waves complementing the recorded information (Figure 3.2b). Refraction seismic data is not as sensitive to reflective structures as reflection seismic data but the data contains more information on the velocity distribution the seismic rays sample. The basic equations for both methods are described for example by Al-Sadi [3].

Within the scope of this thesis near-vertical seismic data was used only when analysing previous models for Moho depth in Paper III and in discussion of the results of Papers I and II.

In Paper II the signal originally tailored for near-vertical reflection experiment FIRE [51] was recorded at wide-angle reflection and refraction distances too, and the obtained data was modelled. FIRE (FInnish Reflection Experiment) was a near-vertical reflection seismic experiment using Vibroseis source, in which the data were acquired in 2001-2003 along 4 transects (Figure 1.2). Of the 4 transects only FIRE4 is situated in northern Finland and our study area, while FIRE1 crosses Kuhmo Greenstone Belt in the study area of Paper 1 and the other two transects are in southern and central Finland. FIRE4 transect consists of two long profiles (FIRE4 and FIRE4A) and shorter FIRE4B profile. The wide-angle reflection and refraction data used in Paper II was recorded along FIRE4 profile. The signal was recorded by 13 portable seismic stations deployed by Sodankylä geophysical observatory of University of Oulu and Institute of seismology of University of Helsinki.

In Paper I the data from SVEKA'81 profile [58, 50] was remodelled concentrating not on the whole crustal scale, as was the original aim of the SVEKA'81 project, but in as good as possible detail in the upper crustal structures close to the target area of Kuhmo Greenstone Belt down to the depth of 20 km. Both in Paper I and II the modelling was done using trial and error method and ZPLOT program [94] for visualising the data and picking the arrival times and SEIS83 program [13, 44] for ray-tracing.

In addition to near-vertical reflection data also available wide-angle reflection and refraction models were analysed for Moho depth information in Paper III.

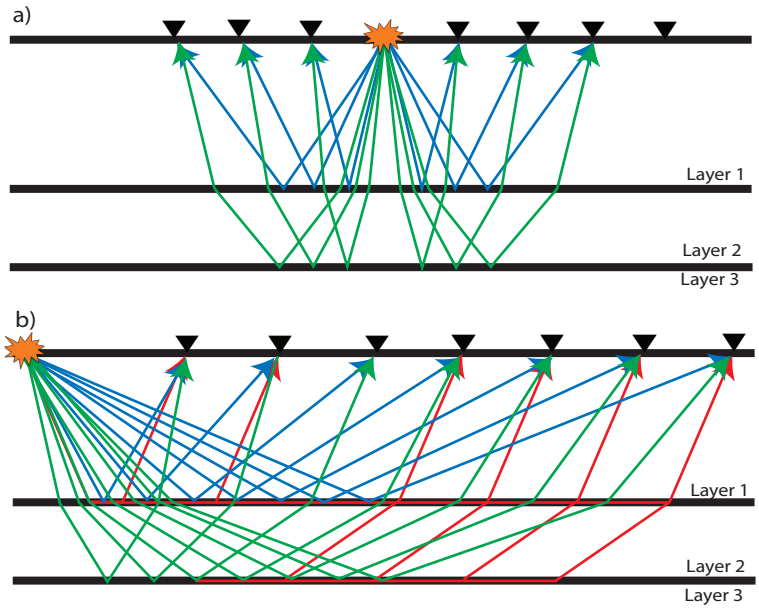

Figure 3.2: The wave phases of the interest in near-vertical reflection seismic survey (a) and wide-angle reflection and refraction survey (b). In both subplots the source is marked with orange explosion and the recording stations with black triangles. The waves reflected at the bottom on the Layer 1 and Layer 2 are marked with blue and green arrows, respectively, and refracted waves are marked with red arrows.

3.2 Receiver function method

Receiver function method is a passive seismic method where the waveforms of the teleseismic body waves are used to image the crustal and upper mantle structures beneath a seismic station. The method is based on the energy converted either from P- to S- or from S- to P-wave energy at the velocity discontinuities below a recording seismic station. While both P- and S-waves can be used to calculate receiver functions, only P-wave receiver functions (PRFs) are considered within the scope of this thesis. In PRF method the interest is in the first arrival P-wave energy converted to S-wave (Ps phase) at lithospheric velocity discontinuities according to Equation (3.4) and the reverberation of the seismic energy between the interfaces and the surface. See Figure 3.3 for an example of some of the possible reverberations. As S-wave velocity is slower than P-wave velocity, the converted phases arrive after the first arrival P-wave. The difference between the P phase and converted phase arrival times depends on the depth of the seismic boundary and the velocity structure above it.

In order to isolate the relatively weak converted phases from seismic recording, the first step in defining a PRF is to rotate the 3-component seismic recording from standard north-south, east-west and vertical coordinate system using either a traditional 2D rotation, where the horizontal components are rotated to the event azimuth coordinate

system of radial (R) and transverse (T) components, or using a 3D rotation to a ray coordinate system (see Figure 3.4 for an illustration depicting the coordinate systems). The coordinate system used in Paper III is Q, T and L coordinate system, where the L component points in the direction of the seismic ray, Q component is perpendicular to L and T is perpendicular to both L and Q components. In ideal case, L, Q and T components contain all the P-wave energy, vertically polarized SV-wave energy and horizontally polarized SH-wave energy, respectively. The advantage of the L, Q, T coordinate system to Z, R, T system is that the P, SV and SH energy is better confined into the respective components. However, presenting the seismic recording in Z, R, T coordinate system is useful for example in seismic anisotropy studies based on PRFs [87, 93].

The azimuth and incidence angle needed for the rotation can be either theoretically calculated using a 1D reference model of the Earth, when the hypocentre of the event is known or they can be measured by particle motion observation of the first arrival P-wave from the data. The latter takes into account possible 3D structures beneath the recording station and was used in Paper III.

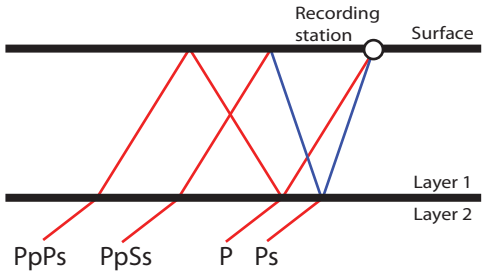

Figure 3.3: A sketch of direct P-wave, the Ps phase as well as some examples of multiples. Red colour denotes P-wave and blue colour S-wave.

After the rotation, the effect of the seismic source has to be removed from the recording to obtain the signal response of the Earth beneath the recording station, the receiver function. It is usually assumed that the first arrival P-wave recording in L component contains the information of the source field. Hence, the spectral division of Q component by L removes the contribution of the source from the recorded Q component. In practice, there are multiple approaches to this, both in frequency and time domains. Widely used techniques in frequency domain are spectral division, commonly used with damping to increase stability, [5] and multi-taper spectral correlation method [63]. The method used in Paper III utilizes a Wiener deconvolution filter, found by minimizing the difference between a normalized spike-like function and the filtered L component, in time domain [88]. To increase signal-to-noise ratio of weak converted Ps phases, PRFs of multiple events recorded by same station are commonly stacked. Finally, the obtained PRF can be inverted to a S-wave velocity model of the crust and upper mantle beneath the seismic station. The in-depth description of the method used in Paper III is found in [40, 47, 88].

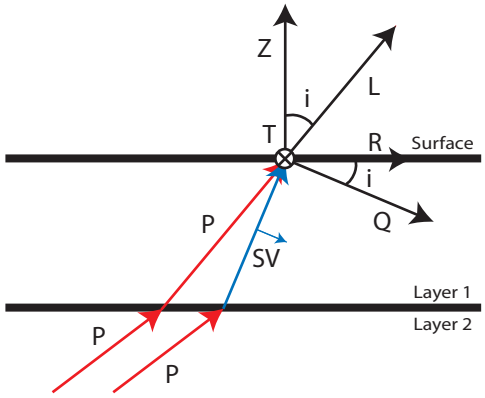

Figure 3.4: The ray coordinate system used in receiver function method. The teleseismic P-waves are marked with red and the converted SV-wave S in blue. Labels Q, L and T represent the axis of the ray coordinate system. The angle i denotes the incidence angle of the first arrival P-wave.

In Paper III the PRFs of POLENET/LAPNET stations were found and inverted to S-wave velocity models and previous PRF models for SVEKALAPKO stations overlapping POLENET/LAPNET study area [49] were analysed for their Moho depths and respective depth estimate uncertainties. The obtained crustal thickness information was used to complement the Moho depth information database compiled from previous CSS models and to build a Moho depth map of the POLENET/LAPNET study area.

3.3 Uncertainty estimation in seismic methods

As both wide-angle reflection and refraction data are commonly forward modelled using trial and error method, there is no inbuilt mathematical error estimation scheme. The goodness of the fit between observed and calculated data is evaluated in qualitative way making the error estimation less straightforward than in inversion-based methods, where some numerical estimates of the quality of the inversion are typically obtained during the inversion procedure (misfit of observed and calculated data and data and model variances). This is the case for example for trial and error modelling of seismic data both in Papers I and II, where the quality of the fit between observed and calculated traveltimes is evaluated solely based on visual comparison of the datasets. The inversion was used side by side with forward modelling in Paper II, and the quality of the fit of the inversion is established numerically as the error estimates of inversion parameters (P-wave velocity grid and the depth grids of the seismic interfaces defined in the model).

In Paper III we concentrated on error estimation of Moho depth information from various different seismic methods. The aim was to obtain reliable crustal thickness

information with comparable uncertainty estimates from as many different previously published seismic models and datasets as possible. The error estimation scheme was based on the scheme proposed by Waldhauser et al. [89]. In the scheme the previously published 2D models are taken and the uncertainty of the data used for each model at Moho depth estimated. The uncertainty estimate of the wide-angle reflection and refraction data is based on the quality of the seismic recording and the visual confidence of recognizing each phase correctly as well as geometric considerations such as profile orientation with respect to known strike directions and the ray coverage. The uncertainty estimate of the near-vertical reflection profiles is similarly based on the quality of the reflective signature, reliability of the migration velocity information and the maximum projection distance of the migrated section from actual true profile.

Each CSS profile was analysed for sections of Moho from where actual data (recorded waves that reflected or refracted at the interface) is available, and each section was given a quality estimate varying between 1 (best data) and 0 (no data). Based on analysis of Fresnel's zones the error of the very best quality CSS data at Moho depth is in scale of ± 2 km [41]. The uncertainties of the located Moho sections were scaled based on this base value in comparison to their respective quality estimate to obtain an error estimate in terms of kilometres.

The uncertainty estimation scheme for PRF inversion results was originally added to the scheme of Waldhauser et al. [89] by Spada et al. [79] and later edited to be more suitable for Precambrian crust in Paper III. In this scheme each Moho depth determined from velocity models based on PRFs was attributed into a predefined quality class and every class was assigned a corresponding uncertainty value. The PRFs were attributed to a quality class based on their record quality (Moho spike sharpness) and certainty of identification of the Moho Ps phase from other Ps phases and noise as well as geometrical considerations. The geometrical considerations include the azimuthal coverage of the seismic events used to obtain the PRF and variations in timing, wavelet width and amplitudes of Ps recordings of individual recoded events with respect to azimuthal direction. These variations could be caused by crustal anisotropy or a 3D structure of the Moho below the seismic station in question, hence increasing the uncertainty of the PRF results.

While the aim of the evaluation process is to obtain error estimates as quantitative as possible, the estimation of the confidence of the refracted and wide-angle reflected phases and of the quality of the reflective signature is still somewhat subjective and, hence, the process remains in parts qualitative.

Chapter 4

Teleseismic traveltime tomography

In seismic tomography the 3D structure of the Earth is studied in a way analogous to methods used in X-ray tomography in medicine and radio astronomy. The early history of seismic tomography is in 1970s when the Earth's average radial velocity structure was already well-established and the general interest shifted to solving lateral variations and later 3D structures inside the Earth [77]. In teleseismic traveltime tomography the data set consists of registrations of seismic signals at teleseismic distances. United States Geological Survey USGS defines the teleseismic distances to be larger than 1000 km.

The velocity variations inside the study volume of a teleseismic traveltime tomography study can be described in various ways but a commonly used method, and the method used in this thesis, is to build a 3D orthogonal velocity with regular horizontal and vertical structure. The velocities between the grid points are interpolated linearly. During the inversion of the traveltime data, the velocity value of each block are optimised to fit the data.

In teleseismic traveltime tomography one handles the traveltime residuals, the difference between recorded and theoretical traveltime, and the ray path inside the study volume, not the actual recorded traveltimes and the whole ray path from the source to the receiver. As the consequence an obtained velocity model does not contain the actual seismic velocities but horizontal velocity variation within each model layer consisting of the blocks at certain depth. While the method uses a preselected reference model as a starting model, the final velocity perturbations are highly averaged to the current average velocity of the layer instead of being directly comparable to the reference model. This condition leads to the main restrictions of the teleseismic tomography namely:

1. There is no way of ascertaining the inverted traveltime perturbations are caused only by the 3D structure of the study volume, even though there are steps in data handling aiming to remove the outside influence. If they are caused by the structures outside of the study volume, they will still be inverted inside.
2. The vertical velocity structure is not obtained but is up to interpretation. The

velocity variations are resolved reliably in horizontal direction only.

Despite these limitations, the method has become a widely used and established technique in constraining the 3D structure within lithosphere and the uppermost asthenosphere [23].

The teleseismic tomography of today is largely based on pioneering work done in California in mid-70s, which led to development of AHC method by Aki et al. [1]. Since then the method has gone through multiple upgrades with advances in computer technology as well as refinements for example in model parameterization (e.g. [42]), 3D ray tracing (e.g. [80]) and inversion algorithms as well as techniques to assess resolution and error (e.g. [22, 75]). Figure 4.1 presents a schematic sketch describing the main features of the method.

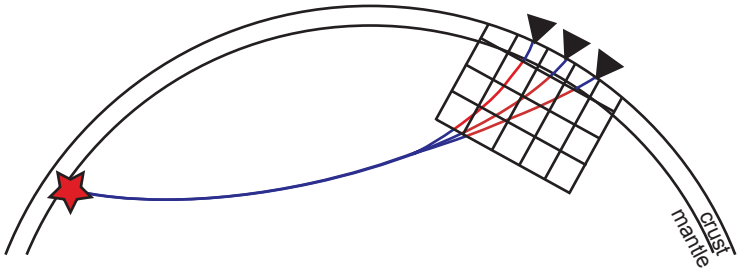

Figure 4.1: The principles of teleseismic tomography. The red star denotes a teleseismic earthquake. Only the part of the traveltime with the seismic ray travelling through the block model (marked with red) of the study volume is used as an input data for the inversion, while the rest of the ray path (marked with blue) excluded using different corrections. The uppermost part of the block model is represented by the crustal correction (see the following Chapter for details) and is not inverted either.

In Paper IV we used TELINV code both for the inversion of the traveltime data and for the forward calculation of traveltimes through predefined velocity models. The program was originally developed by Evans and Achauer [22], and later modified and used by several authors (e.g. [6, 20, 36, 75, 78, 91]). The traveltime calculation is based on the 3D Simplex ray-tracing technique [80].

The basic system of equations to be solved in teleseismic tomography is

$$\mathbf{d} = \mathbf{Gm} \tag{4.1}$$

where $\mathbf{d}$ is a data vector containing N traveltime residuals, $\mathbf{m}$ is a model parameter vector composed of slowness perturbation of each M inversion cells and $\mathbf{G}$ is a NxM matrix defining the coupling between traveltimes and velocity perturbations. In practice G_ij is the distance each seismic ray travels inside a particular cell j and

$$d_i = \sum_{j=1}^{M} G_{ij} m_j. \tag{4.2}$$

TELINV code uses damped least squares method to solve the Equation (4.1). While seismic tomography studies usually have more data than model parameters, in case of real data we deal with data errors as well as inadequacies in the formulation of the inversion model. Additionally thanks to the uneven station and data distribution of a typical real-life seismic tomography problem, some parts of the study area are overdetermined while other parts are underdetermined. For this reason, the exact solution for (4.1) cannot be obtained and the basic inversion equation for TELINV has to be written as

$$\mathbf{m_{est}} = (\mathbf{G^T W_d G} + \varepsilon^{\mathbf{2}}\mathbf{W_m})^{-\mathbf{1}}\mathbf{G^T W_d d}, \tag{4.3}$$

where $\mathbf{m_{est}}$ are estimated model parameters, $\mathbf{W_d}$ is the weighting matrix of the data, ε^2 is a damping factor, and $\mathbf{W_m}$ is the smoothing matrix of the model [60]. As both methods use damped least squares method, the Equation (4.3) is similar to the Equation (2.8) introduced for inversion of Bouguer anomaly data with Grablox in Chapter 2.2.

4.1 Data selection and handling

The first step in teleseismic traveltime tomography is the selection of the recorded earthquakes, the events, used to build the traveltime residual database. One of the basic assumptions of the method is that outside of the study volume the seismic velocities are equal to those of the standard 1D reference model selected for the study. Even though teleseismic distances are defined to begin at 1000 km, the waveforms of seismic events recorded at distances smaller than 30° (roughly 3500 km) mainly propagate through the upper mantle with more complex structure than the deeper portions of the Earth. To simplify the data handling, only events with distances larger than 30° from the POLENET/LAPNET array are selected to the traveltime residual dataset used in this thesis. On the other hand at distances larger than 100° the first arriving P-waves are those that have reached outer core and these events are were excluded from consideration as well.

The other qualifications of a good seismic dataset are well-recorded events with as reliable as possible hypocentre and offset time information. The quality of the inversion benefits from seismic rays arriving into study volume from different directions, which makes a good azimuthal coverage one of the important criteria in selecting seismic events for a teleseismic tomography study.

In Paper IV the events were selected from distances of 30 – 90°. The events were selected from the bulletin of International Seismological Center providing the offset time and epicentre coordinates information. Generally events with magnitude larger than 6.0 were considered but some smaller magnitude but still well recorded events from azimuthal directions with less or no events were added to the dataset.

Defining the first arrival time of seismic signal is called picking the arrival. As the recorded waveform of the P-wave may vary between different sensor types, it is crucial to make sure the first break is measured as reliably as possible [22]. For

POLENET/LAPNET dataset a short period WWSSN simulation filter was used to transform the recordings of different instrumentations to comparable waveform shapes.

One procedure to help defining the first arrivals of poorer quality data is to select a station with good signal-to-noise ratio and compare its waveform to those of the other stations registering the same event. The absolute first break is picked only for the station with best quality recording, called the reference station, while the rest of the recordings are picked at some corresponding peak or through relative to the reference station (see Figure 4.2). Normally the first arrival waveform stays stable across the array, which suggests the bias of picking the relative arrival times (peaks) instead of absolute arrival times (first breaks) is smaller than the possible picking error from picking the absolute first arrivals for poorer quality traces. The quasi-absolute arrival time can be calculated by subtracting the difference between absolute and relative arrival time of the reference station from the relative arrival times of the other stations. When picking the data, each pick was also simultaneously assigned a quality class with accompanying picking error estimate based on the record quality. An example of the data and the picks are shown in Figure 4.2 for all three quality classes.

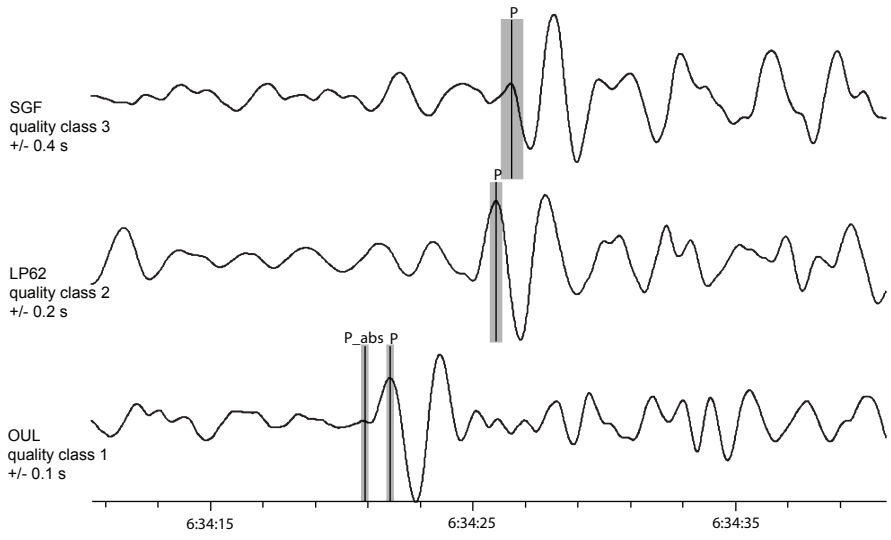

Figure 4.2: An example of POLENET/LAPNET data and the picking results. All three quality classes are shown with their error bars marked with grey rectangle. The absolute traveltime P_abs was picked from the recording of the station OUL in addition to relative travel time P.

The input data for teleseismic traveltime tomography are the traveltime residuals, $\Delta(t)$. To obtain the residual, the observed traveltimes are compared to a traveltime

through a selected reference model

$$\Delta(t) = t_{obs} - t_{ref}. \tag{4.4}$$

The aim is to reduce the traveltime to its anomalous part caused by the velocity variation below the station array and inside the study volume. In Paper IV the reference model was IASP91 [39]. The residuals can still carry some effects from lower mantle heterogeneities and the lithosphere close to source area as well as effects related to errors in event location or timing. As the magnitude of these effects is generally equal at all recordings of a particular event, an effective way to reduce it is to remove the averaged residual over all stations recording the event from the corresponding residuals [22].

The last correction commonly done to the traveltime residuals is the removal of the effect of the crust. Especially the variations in the thickness of the crust can have effects on the traveltime residuals comparable to the velocity perturbations in the upper mantle. These effects have too high magnitude to be modelled with smoothly varying velocity resulting from tomographic inversion and, if they are not corrected, the effect can spread down to the depth of hundreds of kilometres [75]. In Paper IV the Moho depth map defined in Paper III in addition to average P-wave velocity information cleaned from previous CSS studies was used to calculate the crustal corrections.

Figure 4.3 presents the process of obtaining the final residuals of the station LP62 located in central part of POLENET/LAPNET array.

4.2 Model parametrization

The correct selection of inversion and regularization parameters is critical for successful and mathematically stable inversion procedure. The parameters must be selected in a way that allows the inversion Equation (4.3) to be solved to the optimal detail level defined by the qualities of the dataset (mainly station and event distribution). The inversion parameters include both the dimensions of the whole inversion grid and the size of each inversion cell. The regularization parameters include the factors in Equation (4.3): the damping and smoothing, as well as the number of iterations used.

The inversion grid has to be large enough to encompass the whole study volume or the volume where the traveltime residuals are estimated to carry information. If the model is too small, the effect of the velocity perturbations outside is transported into the study volume. The size of the model cells determines the level of details the inversion can achieve. On the other hand the larger the cells the more seismic rays cross each of them and the better the velocity inside each cell is resolved.

In Paper IV the horizontal cell size of 80 km is slightly larger than the average distance between stations in the POLENET/LAPNET array (70 km) to ascertain there are no near surface cells with no ray coverage at all. The study area is a 720 km x 720 km rectangle covering the POLENET/LAPNET study area. In vertical direction the inversion is calculated between the depths of 60 - 450 km with the uppermost inverted layer being 40 km thick, the second 50 km and the rest 5 layers 60 km each. The

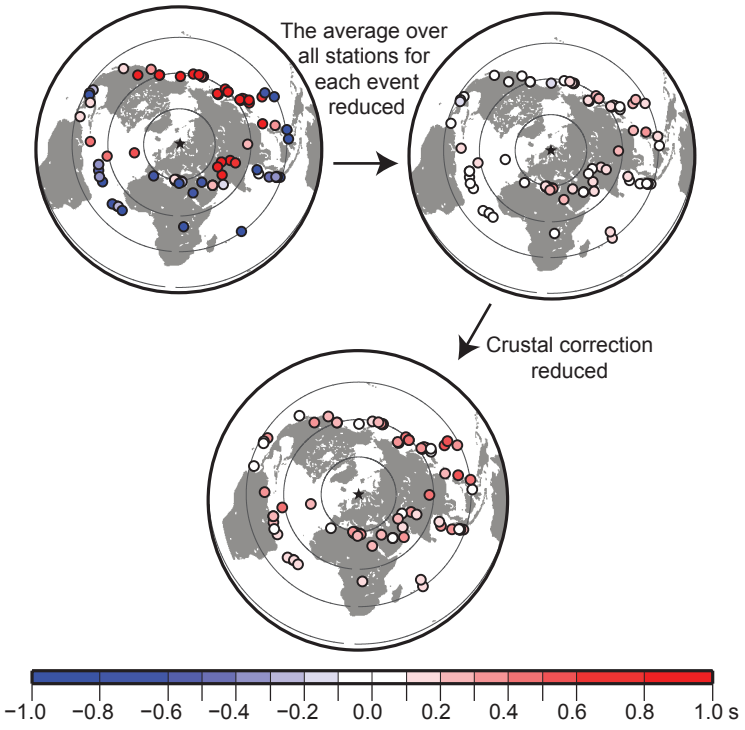

Figure 4.3: An example of the traveltime residuals of POLENET/LAPNET station LP62. The upper left plot shows the initial residuals obtained using Equation (4.4), the upper right plot shows the residuals after the average residual over all stations was removed from each residual and the lower plot shown the residual after removing the crustal correction, too. The residuals in lower plot are those used as a part of the traveltime residual database in Paper IV. The circles inside each plot mark the distances of 30°, 60° and 90° from the station.

IASP91 reference model [39] was used both as the reference model for the calculation of the traveltime residuals and as the velocity distribution of the starting model for the inversion.

The optimal damping parameter and number of iterations are often found by trial-and-error method by running inversion with different damping values and numbers of iterations. The damping affects the balance between the data and model variances: when one grows, the other diminishes. The data variance in the variance of the data values entering the inversion taking into account the uncertainty of the respective quality class of each picked traveltime. The model variance is the variance of the model adjustments done during the iteration. The optimal damping value is commonly selected as the value that yields the optimal balance between the variances. For the dataset and model grid used in Paper IV the damping was set to 70 after careful

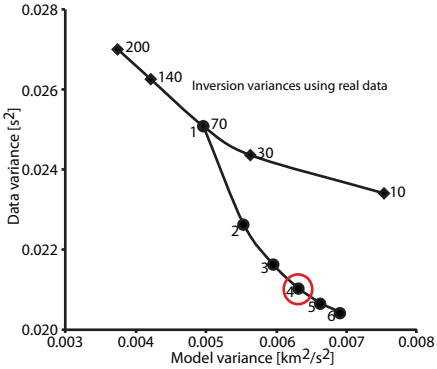

Figure 4.4: The trade off curve of the data and model variances for POLENET LAPNET teleseismic tomography inversion presented in Paper IV. The tests using different damping values are marked with diamonds with the corresponding damping on right. After the damping value 70 was selected, the optimal number of iterations was found. The number of iterations tests are marked with dots with the corresponding number of iterations on left. The results with regularisation parameters selected for the final inversion (damping 70 and 4 iterations) are marked with the red circle.

analysis. While testing the number of iteration, we found that after 4 iterations the changes in the model and the variances are insignificant. See Figure 4.4 for the trade off curves between model and data variances for the damping and the number of iterations. The quality of the inversion parameters and the grid was tested using resolution tests described in following section.

4.3 Model resolution assessment

One important question left to answer is the reliability of the inversion results. There is no direct information (e.g. borehole data) from upper mantle depths available to compare the results to, which makes the analysis of resolution capabilities of the dataset and the inversion grid crucial. The inversion quality depends not only on the quality of the data and the inversion software but also on the choice of the inversion grid and regularization parameters. There are several ways of assessing the resolution capabilities of teleseismic tomography data, e.g. hit matrix, derivative weighted sum, ray density tensor, resolution matrix, and synthetic tests [75]. In Paper IV the resolution and sensitivity were estimated analysing the diagonal elements of the resolution matrix and synthetic tests.

Both checkerboard tests and other synthetic tests are so called model restoration tests (e.g. [42]). A theoretical traveltime residual dataset is calculated by tracing the rays through prebuild velocity perturbation model. Some random noise is commonly added to simulate a real dataset. Synthetic traveltime residuals are calculated using ray tracing through the input model, while the other parameters for each seismic ray (recording station coordinates, back-azimuth direction and the ray parameter) stay

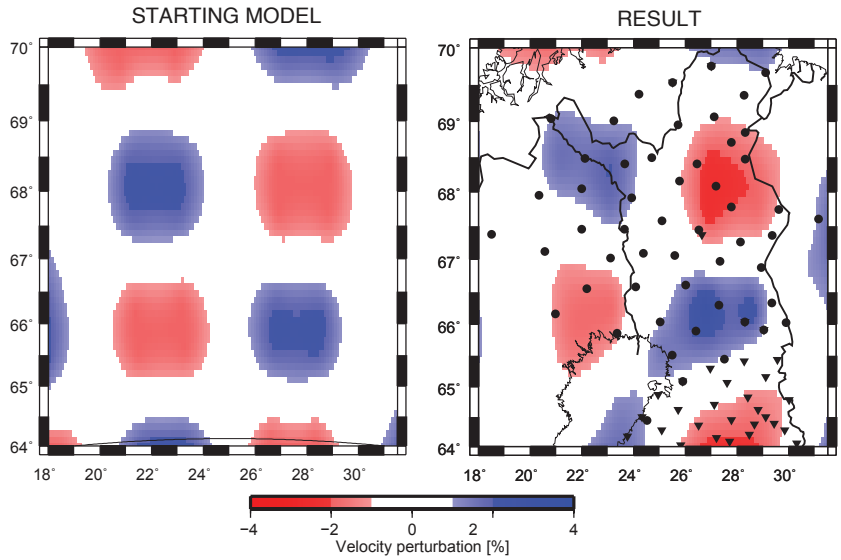

Figure 4.5: Example of the results of a checkerboard test at the depth of 120 km. The model used to calculate the synthetic dataset is on the left and the recovered anomalies after the inversion of the synthetic dataset is on the right. The black dots and triangles mark the locations of POLENET/LAPNET and SVEKALAPKO stations, respectively.

the same as for the real dataset to simulate the station and data distribution of the real data as closely as possible. Similarly, the same model grid and regularization parameters are used. Finally the obtained theoretical database is inverted and the inversion results are compared to the model used to calculate the theoretical data to see how well the test structures are recovered.

In classical checkerboard tests the theoretical model is filled with alternating positive and negative anomalies in both horizontal and vertical directions [75]. Figure 4.5 shows an example of checkerboard test results. Other synthetic tests might include hypothetical velocity structures based on *a priori* information (as in Paper IV) and/or they may be build to specifically test the sensitivity of the dataset in selected part of the study volume [42].

In addition to sensitivity tests the resolution of the inversion was estimated by analysing the diagonal elements of the data resolution matrix. The resolution matrix describes the capabilities of the ray geometry and model parameter grid to resolve the velocity perturbations [60] and can be defined as:

$$\mathbf{R} = (\mathbf{G^T W_d G} + \varepsilon^2 \mathbf{W_m})^{-1} \mathbf{G^T W_d G}. \tag{4.5}$$

While the whole resolution matrix would describe the overall resolution capability of each inversion cell with respect to each cell of the model, the diagonal elements give an estimate of the general resolution in that cell [60]. The larger the diagonal element,

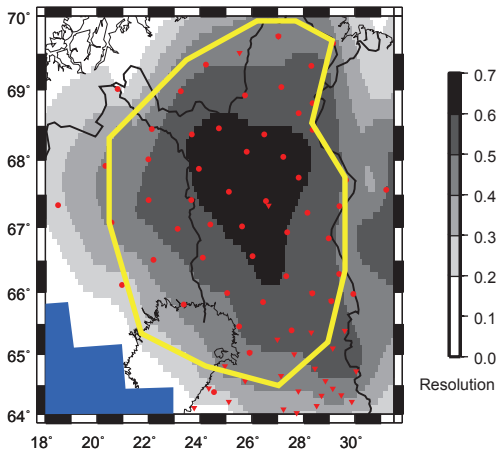

Figure 4.6: A map of the diagonal elements of the resolution matrix. The red dots mark the locations or POLENET/LAPNET seismic stations and the triangles mark SVEKALAPKO stations. The region marked with blue was excluded from inversion, as there was no ray coverage at all. The area surrounded by the yellow line shows the region of fairly good resolution.

the better the corresponding model parameter is resolved. If the diagonal element has a small value, the corresponding inversion cell cannot be resolved well independently but its value is tied to those of the surrounding cells. Figure 4.6 shows an example of the diagonal elements of the resolution matrix of an inversion. For the results of the inversion, see Figure 5.8

Chapter 5

Summary and the main results of the papers

5.1 Papers I and II: Gravity modelling and inversion of ore potential belts

Paper I presents 3D trial-and-error modelling and inversion results of Bouguer anomaly data describing Archaean Kuhmo Greenstone Belt in the southeastern part of the study area (See Fig. 1.1). Archean greenstone belts, Kuhmo Greenstone Belt included, often host gold and other valuable metal deposits. Prior to the study, the surface geology of the belt was relatively well known but its 3D structure was not. Also the formation of the belt was debated. The main competing theories were igneous rocks derived from upwelling mantle plume in intracratonic rift environment [59] and a collision and subduction-like processes [67, 81, 82].

On surface the belt is a thin north-south aligned mafic body. It divides the surrounding Archaean basement into two domains with different geological and geophysical properties. The main dataset used in this study was the Bouguer anomaly data of the Finnish Geodetic Institute (compiled by the Geological Survey of Finland) in 10 km x 10 km grid [45, 21, 37]. The belt is clearly visible in Bouguer anomaly data (Fig. 5.1), but not at all in the models of crustal scale seismic datasets crossing it, namely the wide-angle reflection and refraction profile SVEKA'81 [58, 50] and the near-vertical reflection profile FIRE1 [51]. From the available analysis of petrophysical properties of the rock samples we found that the rocks forming the belt have higher density but slightly lower Vp and Vs than the rocks surrounding the belt because of higher amphibole, biotite and muscovite content.

The average density of the rocks of the belt was found using Monte Carlo simulation of petrophysical constraints based on modal mineralogy of the Kuhmo Greenstone Belt. The average density value found by the simulation, 2.84 g/cm^3, was used as the density of the belt in trial-and-error modelling. In addition to the forward modelling, different tests on inversion of Bouguer anomaly data were done to help us evaluate the reliability of the modelling and inversion. As a starting model for both the trial-

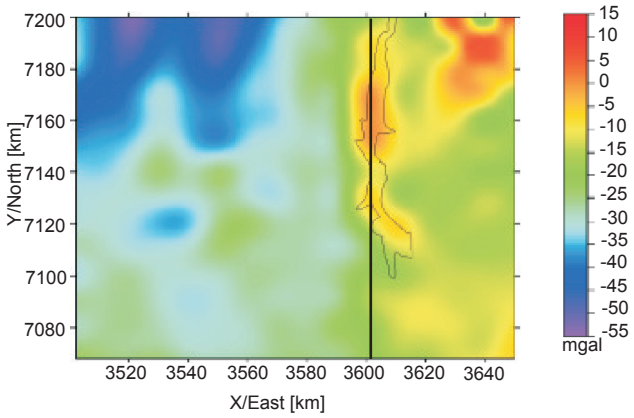

Figure 5.1: The location of the Kuhmo Greenstone Belt on the Bouguer anomaly map of the research area [45]. The Bouguer anomaly map used in this study is defined on 10 km x 10 km regular grid.

and-error modelling and the inversion we used a previous 3D crustal scale density model of southern and central Finland by Kozlovskaya et al. [48]. The results of modelling and inversion consistently suggested a shallow, less than 7 km deep, upper crustal structure with no "root" in middle or lower crust (Fig. 5.2). Combined with the significant change in crustal thickness from 60 km to 50 km at SVEKA'81 model below the belt [50], results seemed to suggest the accretionary origin as the correct one.

Paper II presents P-wave velocity model based on wide-angle reflection and refraction recordings acquired as a complimentary study of Vibroseis signal originally intended for the near-vertical reflection seismic profile FIRE4 [65]. FIRE4 profile is located in Archaean crust reworked in Early Proterozoic (see Fig. 5.3). It crosses Peräpohja Schist Belt in its southern part, Central Lapland Granitoid Belt in the centre and ends at Kittilä Greenstone Belt in its northern end. Both Peräpohja Schist Belt and Kittilä Greenstone Belt are ore potential [19] and are clearly visible in Bouguer anomaly data. In addition to the positive anomalies associated with the belts, a Bouguer anomaly maximum can be seen inside the Central Lapland Granitoid Complex with no obvious explanation on the geological maps.

The seismic dataset was analysed using both forward ray-tracing and inversion to obtain 2D models along the profile. The quality of the recording enabled us to build a model of the upper crust down to the depth of 6 km. To get additional constraints for our P-wave velocity models we complemented the study with independent 3D gravity inversion and modelling of the study area. In gravity inversion we used Occam inversion with available petrophysical density information from the surface as *a priori* information.

The main surface geological units can be recognized from both seismic and gravity models. Of the units of higher P-wave velocity and density Peräpohja Schist Belt

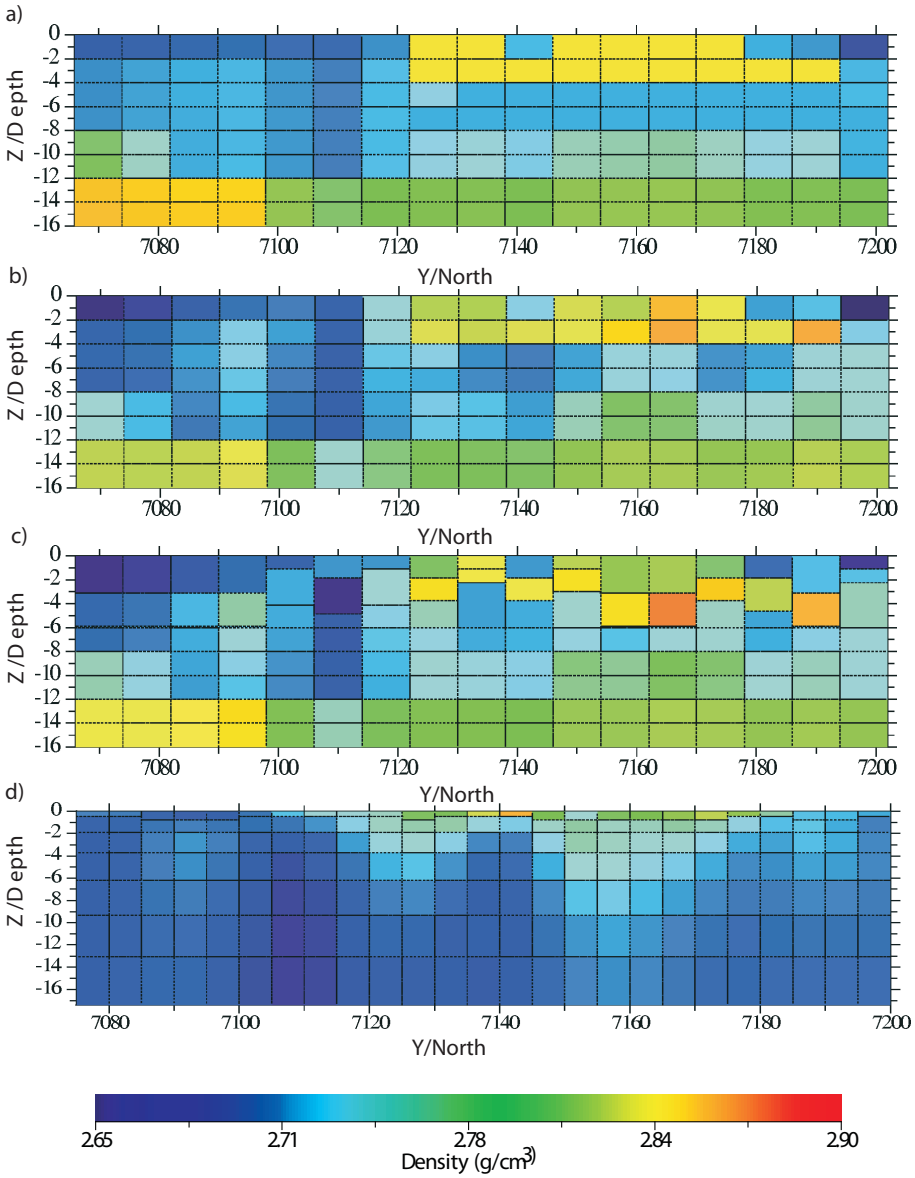

Figure 5.2: Example vertical sections through modelling and inversion results. Subplot a) shows a trial-and-error model, subplot b) the inversion results with density optimisation, subplot c) the results after height and subsequent density optimisation, and subplot d) the resulting model obtained by the Occam inversion.

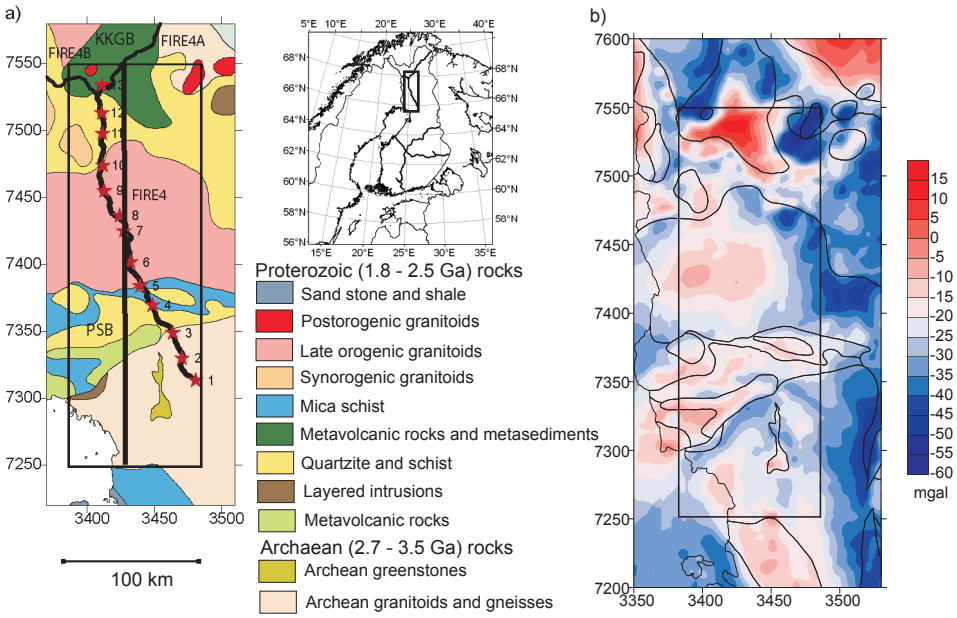

Figure 5.3: Subplot a) shows the geological map of the study area of Paper II based on [43]. The rectangle shows the gravity inversion study area and the thick black line denotes the location of section through 3D density models on Figure 5.6. FIRE transect is marked on the map on black and the receivers of the wide-angle reflection and refraction study are shown as red stars. The geological units marked on the map are PSB – Peräpohja Schist Belt and KKGB – Karasjok-Kittilä Greenstone Belt. Subplot b) shows the Bouguer anomaly map of the study area [43] defined on 10 km x 10 km regular grid.

seems to extend only to the depth of few kilometres while Kittilä Greenstone Belt seems to be deeper than 8 km extent of our model, although the model suggest that the base of the belt might almost be reached. Based on regional scale model by Janik et al. [35] the Greenstone Belt does not extend deeper than 10 km. In addition we found a high P-wave velocity anomaly at the location of a positive Bouguer anomaly in gravity data. This body was modelled both with gravity and seismic methods to the approximate depth of 4 – 6 km and its origin is unknown. While the density obtained during Bouguer anomaly inversion and modelling may indicate granodioritic or metasedimentic composition, the highly reflective nature of the body in FIRE4 profile implies strongly deformed and folded rocks with contrasting elastic properties. The nature of this sub-surface body can be potentially interesting for further studies, including origin of the mineral system in the area. Figure 5.4 summarises the main result of both seismic and gravity modelling and inversion.

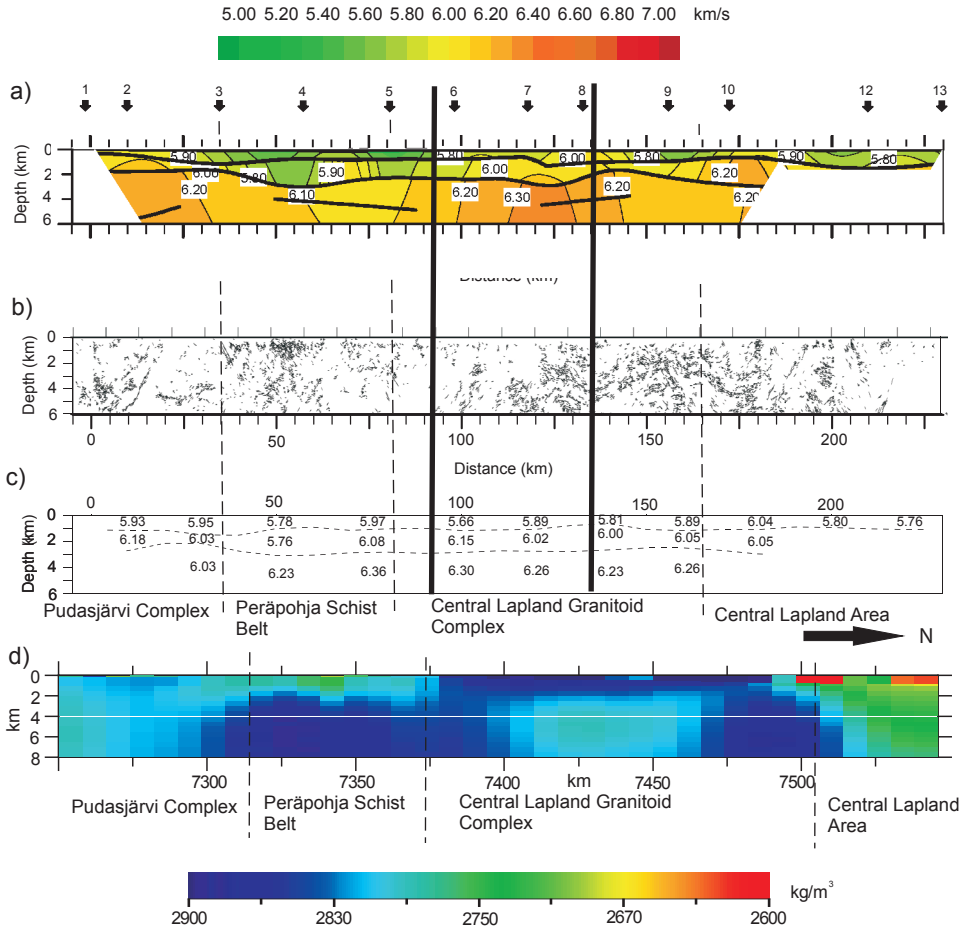

Figure 5.4: Subplot a) shows a trial-and-error ray tracing model of FIRE4 wide-angle reflection and refraction data. The receiver locations are marked with arrows above the model. Subplot b) shows an automatic line drawing of the near-vertical reflection profile FIRE4 after Patison et al. [65] and subplot c) a seismic inversion model of FIRE4 calculated using Rayinvr software. Subplot d) shows a section through 3D density model obtained using Occam inversion. The main geological units are marked below the figures and their boundaries are marked with dashed line throughout all models. The horizontal limits of the high density body from the gravity inversion is marked through the seismic sections with thick black lines. See Figure 5.3 for the location of the seismic models and the density section.

5.2 Papers III and IV: New Moho depth map and crustal correction model

Paper III presents a regional scale study of crustal thickness in northern Fennoscandian Shield. The aim of the study was to build an updated 3D crustal model of POLENET/LAPNET study area (see Fig. 5.5) to be used as a crustal correction for upper mantle studies (for example Paper IV). The study was based on previously published controlled source seismic profiles in the area and previous and new receiver function results. The main controlled source seismic profiles used were wide-angle reflection and refraction profiles FENNOLORA [28, 29, 57], POLAR [35, 56], and PECHENGA-KOSTAMUKSHA [7, 8, 9], and a near-vertical reflection transect FIRE4 [35, 65]. The profiles were complemented by some shorter profiles, most of them 1D. The available receiver function results were previously defined receiver functions of northern stations of SVEKALAPKO array [49] in southern part of the study area and new receiver functions based on POLENET/LAPNET data defined as a part of this study. See Fig 5.5 for the locations of the controlled source seismic profiles and the receiver function stations.

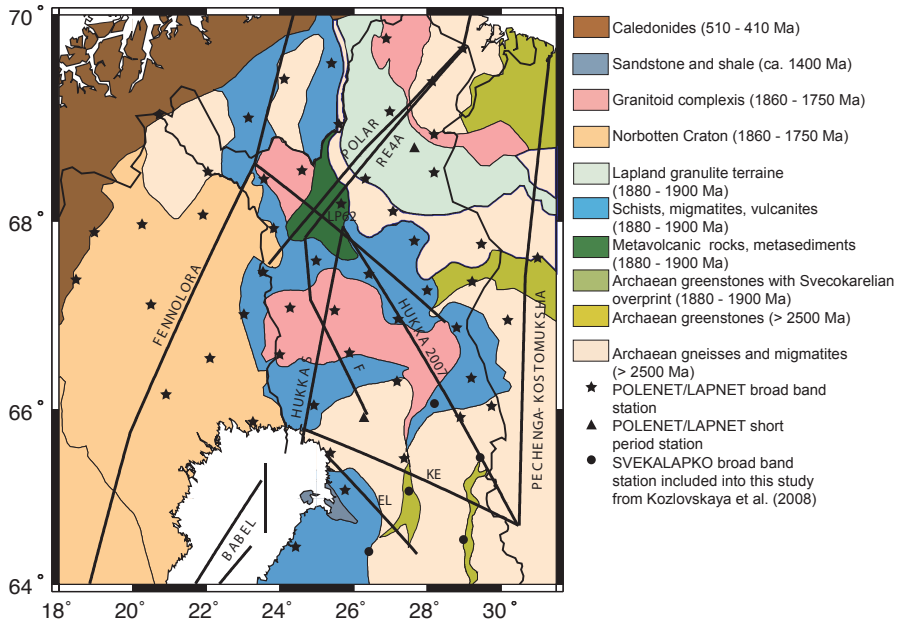

Figure 5.5: The simplified geological map is based on a 1:2000000 geological map of Fennoscandia [43]. The controlled source seismic profiles used as input data in Paper III are indicated with black lines and the receiver function points with black symbols.

For each dataset the locations of actual Moho information were found by analysing the published models and data (see the secments of actual Moho inforamtion in Fig. 5.6. For each Moho segment of Moho depth information also an individual error

estimate was found using the error estimation scheme proposed by Waldhauser at al. [89] for controlled source seismic data and updating the scheme by Spada et al. [79] for receiver functions. The schemes are based on the strengths and weaknesses of each seismic method and the properties of the data set and enabled us to compare models obtained using different seismic methods. The error estimation scheme is shortly described in Chapter 3.3.

The result of the study was an updated Moho map of Northern Fennoscandian Shield. The average crustal thickness in the study area is 45 km. The map can be divided into three main domains with eastern and southwestern domains having shallower Moho on average at 42 km depth and the region in between with having deeper Moho (on average 47 km). Especially from PRF results we can see that the Moho signature below the shallower domains is generally simple and clear while the signature below deeper part tends to have wider Moho conversion pulse, often a clear combination of two or three pulses, in the RF signifying a complex structure of the Moho boundary.

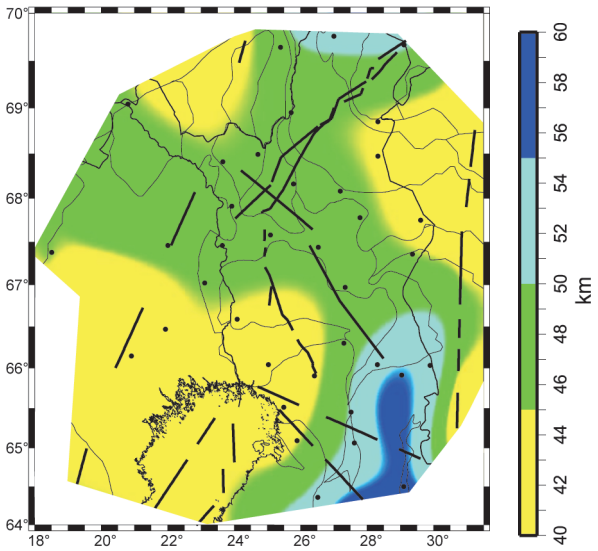

Figure 5.6: The Moho depth map obtained in Paper III together with a simplified map of geological units (based on [43]) and the locations of controlled source seismic and receiver function Moho information.

The main locations where the map differs from previous maps (e.g. [27, 55, 46, 83]) are the southeastern and northeastern corners of the study area, where pronounced Moho depressions are found in the new map. The northeastern Moho depression is located in Kola Province and the southeastern one in Archaean part of Karelian Province. The southern Moho depression seems to be a continuation of the deep Moho of central Finland towards north and its thin shape might suggest tectonic origin, which is

supported by the findings of Paper I in the upper crust in southernmost corner of the new Moho map. Both Moho depressions are located in areas where there are no good quality CSS data at Moho depth but the southeastern depression is seen in the PRFs calculated of SVEKALAPKO [4, 49] and POLENET/LAPNET data. In northeastern part of the study area the deeper Moho is supported by both the reflection seismic FIRE4A profile [35] and the PRFs based on POLENET/LAPNET data.

To correct the teleseismic traveltime residual dataset for the crustal effect in Paper IV we build a quasi-3D P-wave velocity model of POLENET/LAPNET study area. From the analysis of the previously published CSS datasets we found that the amount of reliable seismic velocity information was not sufficient to be built into a high precision 3D P-wave velocity model of the whole study area. All major profiles in northern Fennoscandia were more or less in north-south direction and there was almost no velocity information between the profiles to help tie the datasets together and to estimate the continuation of anomalous structures in 3D.

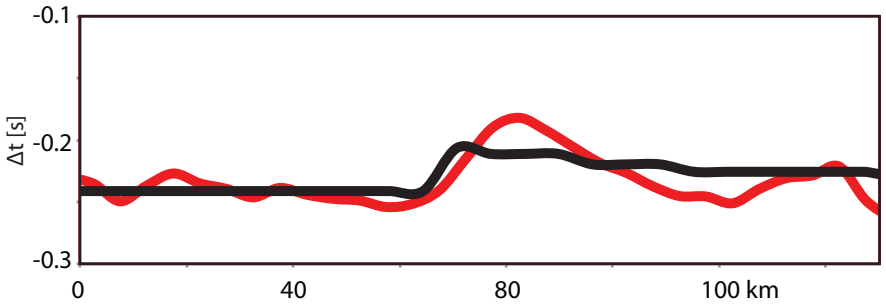

Figure 5.7: A comparison between the vertical traveltime through the crustal correction model used in Paper IV (black) and the wide-angle reflection and refraction model by Janik et al. [35] (red) along southern half of POLAR profile.

The crustal thickness of the quasi-3D velocity model is based on the Moho depth map published in Paper III. The model extends down to 60 km to accommodate all Moho depth variations inside the study area. The velocities inside the crustal part of the model are laterally homogenous and are based on the average P-wave velocity at the depth through the three major wide-angle reflection and refraction profiles located inside POLENET/LAPNET study area (FENNOLORA [29], POLAR [35] and PECHENGA-KOSTOMUKSHA [9]). The P-wave velocity below the crust was set to 8.05 km/s, which is the P-wave velocity of the uppermost mantle of IASP91 reference model ([39]. We found that the differences in the vertical travel time through this model and the CSS models with lateral velocity variations were minor especially when compared to the effect of Moho depth variations throughout the study area. The largest difference seen in comparison with a recent POLAR model [35] is 0.03 s while the crustal correction value varies between 0 and -0.35 s within POLENET/LAPNET study area and the average picking uncertainty of the teleseismic traveltime dataset was estimated to be 0.13 s. Figure 5.7 presents a comparison of the vertical traveltime through the central part of the POLAR profile and the quasi-3D model.

5.3 Paper IV: Teleseismic traveltime tomography model of the upper mantle

Paper IV presents a regional scale upper mantle study in POLENET/LAPNET study area (see Figures 1.1 and 5.5), which is considered to be a prospective source for diamondiferous kimberlitic rocks. Recordings of teleseismic events can be used to explore the mantle lithosphere to the depths of several hundreds kilometres as described in Chapter 4. Earlier Plomerová et al. [72] and Vinnik et al. [87] used POLENET/LAPNET data to estimate seismic anisotropy and Vinnik et al. [86] used receiver function method to estimate the average velocity in the upper mantle beneath the POLENET/LAPNET study area. Our study complements these previous studies by using body-wave tomography technique.

To build a traveltime residual dataset for the inversion, 96 well-recorded teleseismic events were selected from POLENET/LAPNET data acquisition period, picked for P-wave first arrival times and processed into a traveltime residual database using IASP91 reference model [39] and the crustal corrections based on the new crustal model defined in Paper III. The events have a good azimuthal coverage; the largest back-azimuth gap is smaller than 15°. The new P-wave traveltime residual dataset of POLENET/LAPNET array was complemented adding residuals recorded by the northern stations of SVEKALAPKO array overlapping POLENET/LAPNET study area.

The resolution of our dataset and model parameters was studied using classic checkerboard tests, other synthetic tests and analysis of diagonal elements of the resolution matrix. The analysis reveals a reasonably good resolution down to the depths of approximately 400 km below the central part of the array. The main feature seen in final inversion model is a low velocity zone of roughly -3.5% in the central part of the study area. The low velocity zone is surrounded by high velocities beneath the three cratonic components: Norrbotten Province in west (+1.5%), Kola Province in northeast (+3.5%) and Karelian Province in southeast (+3.0%). All the anomalies extend from below Moho to the depth of 160 – 200 km. The structures differs significantly from the mantle revealed by teleseismic tomography beneath SVEKALAPKO study area in central and southern Finland, as well as the mantle models of southern Sweden [78] and some other shield areas around the world [64, 74, 85], where the mantle is characterized by a high velocity lithospheric root. On the other hand, where the study areas of POLENET/LAPNET and SVEKALAPKO overlap the models generally agree even if the overlapping area is not within the best-resolved region of either project.

The lateral variation in velocity perturbations between the non-reworked cratonic lithosphere and the slow velocity zone in the middle is larger than 5%. In general the upper mantle anomalies can be caused by lateral temperature variations, compositional variation or anisotropy. The seismic anisotropy of POLENET/LAPNET study area has been studied by Plomerová et al. [72] and Vinnik et al. [87]. Neither study indicated vertical anisotropy, which would significantly affect the traveltimes of near vertical seismic rays studied in teleseismic tomography, leaving temperature

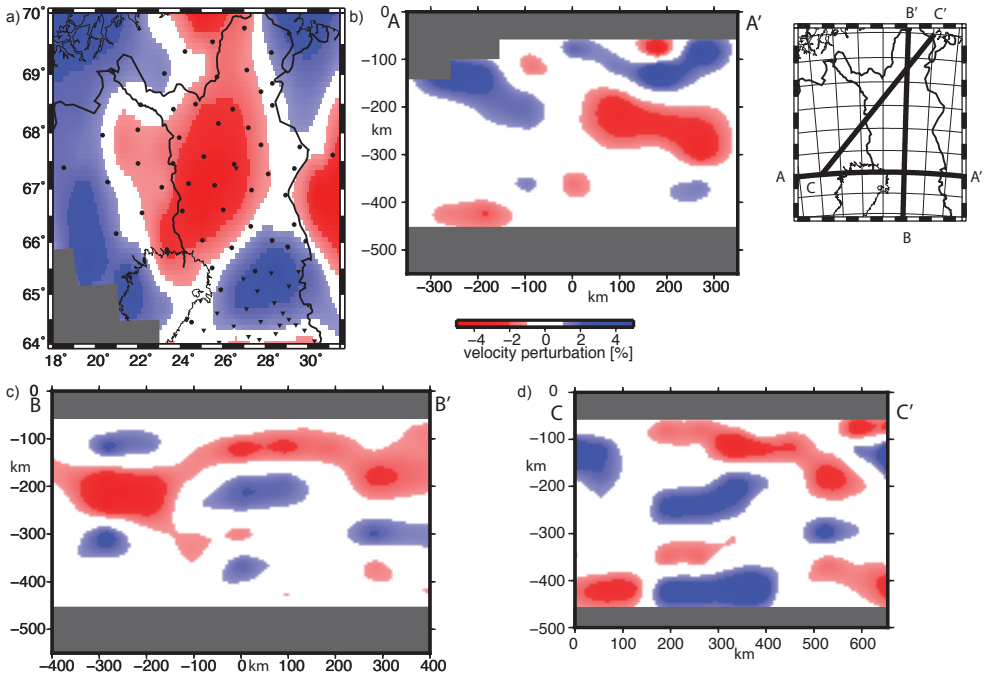

Figure 5.8: The results of the 3D teleseismic tomography inversion introduced in Paper IV. Subplot a) shows a horizontal section through the 3D model at the depth of 120 km. Subplots b) – d) show three vertical sections through the model. The locations of the sections are marked to a small map in upper right corner with thick black lines.

and compositional variation as the most likely sources of the anomaly. While teleseismic traveltime tomography does not resolve well absolute velocities, the simultaneous receiver function study by Vinnik et al. [86] presents significantly lower seismic velocities in the mantle beneath northern Finland, when compared to results for stations located in southern Finland, which supports our findings.

The western part of the low velocity zone between Norrbotten and Karelian Provinces is located below Baltic-Bothnia Megashear marking the boundary between the cratonic units. The low velocity zone can be followed into the adjoining part of the shear zone in the models of the upper mantle based on SVEKALAPKO data [12, 75], where the slower velocities are explained by refertilised composition of the lithospheric mantle. On the other hand the eastern part the zone is co-located with Kola alkaline province [17], in which the crust has been intruded by alkaline magmas during several metasomatic events from Proterozoic to Devonian. The same events would likely result in reworking and refertilisation of the depleted Archaean upper mantle seen in southern Finland [75].

As shown for example by [34, 54, 76], the compositional variations can explain up

to 1-2% velocity variations. Even when taking into account the possible effect of selected inversion parameters to the anomaly magnitudes, it is unlikely the total lateral velocity variation seen in our results could be explained by compositional variations only; additional higher temperatures are needed. In eastern part of the study area the latest magmatic event in Devonian [17] could explain the higher temperatures in mantle, too, but in the western part of the slow velocity zone the existence and timing of the possible thermal event is more speculative.

Chapter 6

Concluding remarks

6.1 Discussion and conclusions

This thesis presents 3D geophysical studies both in ore belt scale (roughly 100 km in horizontal directions and 10 km in vertical dimension), and in regional scale of 700 km x 700 km horizontally with depth extend varying from crustal scale (60 km) to upper mantle scale (60 km to 400 km). The ore belt scale studies are based on controlled source seismic (CSS) data and models and the Bouguer anomaly data of Finland. The regional models are based on CSS data and models and the data of the passive seismic POLENET/LAPNET and SVEKALAPKO arrays. The general conclusion of all four studies is that the 3D structures seen in crust and upper mantle reflect the complex and long geological history of the study area.

Papers I and II present two case studies using Bouguer anomaly data together with available seismic and petrophysical constraints to estimate the 3D density structure of interesting ore potential geological formations. In Paper I the main target is Kuhmo Greenstone Belt, a surface feature, but in Paper II on of the targets was initially visually selected from Bouguer anomaly data and later confirmed independently by both wide-angle reflection and refraction study and 3D Bouguer anomaly inversion, is located below surface at the depth of approximately 2 km. All the formations considered ore potential in the study areas of Papers I and II: the Archaean Kuhmo Greenstone Belt and the Early Proterozoic Peräpohja Schist Belt and Kittilä Greenstone Belt, were found to be relatively shallow structures with depth extent not exeeding 7 km, 3 km and 10 km, respectively. Both Paper I and Paper II demonstrate the advantage of gravity inversion when the Bouguer anomaly data is combined with *a priori* information from petrophysical and seismic datasets. While the block model results of the inversion of the regional scale Bouguer anomaly data may not be sensitive enough for high precision modelling, the obtained models give a good first approximation to support geological datasets when building a geodynamic model of the region.

Paper III presents an updated Moho depth map for the POLENET/LAPNET study area based on previously published CSS and new and previous P-wave receiver function (PRF) results. The map reveals three different crustal domains: in southwest and

east the Moho is flat and relatively shallow (on average 42 km), which is close to the global average for Archaean crust [61], while in northern and central part the Moho is deeper (on average 47 km), which suggest Early Proterozoic origin. The converted Ps recordings of the Moho in receiver function data shows usually a simple sharp pulse in the region with shallower Moho but a complex pulse often formed as a superimposed signal of two or three pulses, suggesting thicker and complex Moho boundary. It is worth noting that the significant number of known ore deposits especially in Sweden but also in Finland are located slightly north of the Moho deepening. Additionally we found pronounced Moho depressions in northeastern and southeastern corners of the study area. Especially in southeastern corner below Archaean Karelian Province, the Moho depth extends down to almost 60 km. The Moho depression seems is be a narrow continuation of the deep Moho of central Finland towards north and it is surrounded from both east and west by shallower (44 km deep) Archean crustal units. The high level of Moho topography in the area suggests tectonic origin, which is supported by the upper crustal results of Paper I.

The upper mantle structures revealed by teleseismic tomography method in Paper IV show a mantle very different from that revealed by SVEKALAPKO data beneath southern and central Finland. While the model of the upper mantle below SVEKALAPKO array [75] is characterized by a high velocity root, the teleseismic tomography results presented in Paper IV reveal high velocities only beneath the three cratonic units in west, southeast and northeast and slower velocities in the central part separating the cratonic units. All the anomalies extend from below Moho to the depth of 160 – 200 km. We interpret the high velocity anomalies to represent a non-reworked depleted Archaean cratonic lithosphere similar to that interpreted below southern and central Finland [75]. The seismic lithosphere is estimated in numerous previous studies to be at least 200 km thick (e.g. [53, 66, 70]) and we find it unlikely the low velocity zone in the central part of the study area is the lithosphere-asthenosphere boundary (LAB). Instead we interpret the zone to represent velocity variations in lithosphere. The generally lower seismic velocities in the uppermost mantle of northern Finland when compared to southern Finland are confirmed by a recent receiver function study [86].

The source of the low velocity zone in the uppermost mantle is still speculative. The zone overlaps in the east with Kola alkaline province with latest magmatic event in Devonian. The western part of the zone in located below Baltic-Bothnia Megashear separating cratonic components of Norrbotten and Karelian Province. The most likely cause of the lower velocities is refertilisation of the mantle during a metasomatic event. Even though the lateral velocity variations in teleseismic tomography are to some extend governed by the inversion parameters, the velocity variation seen in our model is significantly higher (5%) than what can be explained purely by chemical composition (1-2%) suggesting additional explanation of either anisotropy or temperature variation. As there is no indication of vertical anisotropy affecting almost vertical teleseismic rays in previous anisotropy studies of the POLENET/LAPNET data [72, 87], we speculate higher temperature is needed. While a Devonian magmatic event in Kola alkaline province [38] could explain the increased temperature in eastern part of the low velocity zone, there is no obvious candidate for the tectonothermal event in the

western part.

6.2 Recommendations for future research

The work presented here is build around POLENET/LAPNET study area centred in northern Finland. A temporary seismic network SCANarray is currently measuring in Norway, Sweden and Finland. When the data is available, a comprehensive study covering whole Fennoscandian Shield can be done by combining the datasets of the passive seismic arrays in Fennoscandian Shield: POLENET/LAPNET, SVEKALAPKO, TOR and SCANarray. The product of combined datasets makes it possible evaluate the crustal and mantle structures covering whole Fennoscandian Shield making it possible to answer not only the questions raised by the differences of the upper mantle models of southern and northern Finland (SVEKALAPKO and POLENET/LAPNET, respectively) but also to shed further light into the evolution of the Shield as a whole. Additionally the now existing seismic models based on POLENET/LAPNET data can be used to further study the mantle composition in 3D and possibly even 4D and hence speculate on the still unknown mineral and diamond potential of the region.

In crustal scale the existing 3D density model of southern and central Finland [48] can be extended north to cover whole Finland using the Moho map presented in Paper III and rough velocity information cleaned from CSS models in the region as well as Bouguer anomaly data. This model could be used as a regional model for further smaller scale 3D models of Greenstone Belts and other ore potential regions. Comparing the structure of the belts can be used to speculate on the geodynamical evolution of the selected regions. Bouguer anomaly inversion in crustal scale might also help in updating the quasi-3D seismic velocity model introduced in Paper IV to a fully 3D model.

Bibliography

[1] K. Aki, A. Christoffersson, and E. Husebye. Determination of the three-dimensional seismic structure of the lithosphere. *J. Geophys. Res.*, 82:277–296, 1977.

[2] K. Aki and P.G. Rickhards. *Quantitative seismology, theory and methods*, volume 1. W. H. Freeman and Company, 1980.

[3] H.N. Al-Sadi. *Seismic Exploration*. Birkhäuser, 1982.

[4] A. Alinaghi, G. Bock, R. Kind, W. Hanka, K. Wylegalla, and TOR and SVEKALAPKO Working Groups. Receiver function analysis of the crust and upper mantle from the North German Basin to the Arhaean Baltic Shield. *Geophys. J. Int.*, 155:641–652, 2003.

[5] C. J. Ammon, G. E. Randall, and G. Zandt. On the nonuniqueness of receiver function inversions. *J. Geophys. Res.*, 95:15303–15318, 1990.

[6] R. Arlitt, E. Kissling, and J. Ansorge. Three-dimensional crustal structure beneath the TOR array and effects on teleseismic wavefronts. *Tectonophysics*, 314:309–319, 1999.

[7] I. Azbel and V. Ionkis. The analysis and interpretation of wave fields on Soviet and Finnish DSS profiles. In H. Korhonen and A. Lipponen, editors, *Structure and dynamics of the Fennoscandian lithosphere*, pages 21–30. Institut of Seismology, University of Helsinki, 1991.

[8] I. Azbel, A. Yegorkin, V. Ionkis, and L. Kagaloval. *Pecularities of the Earth's crust deep structure along the Nikel-Umbozero-Ruchýi profile, Investigation of the Earth's continental lithosphere with complex seismic methods*. Institut of Mines, St. Petersburg, 1991.

[9] I.Y. Azbel, A.F. Buyanov, V.T. Ionkis, N.V. Sharov, and V.P. Sharova. Crustal structure of the Kola-Peninsula from inversion of deep seismic-sounding data. *Tectonophysics*, 162:78–99, 1989.

[10] BABEL Working Group. Integrated seismic studies of the baltic shield using data in the gulf of bothnia region. *Geophys. J. Int.*, 112:325–343, 1993.

[11] R. Blakely. *Potential Theory in Gravity and Magnetic Applications*. Cambridge University Press, 1996.

[12] M. Bruneton, H.A. Pedersen, V. Farra, N.T. Arndt, P. Vacher, and SVEKALAPKO Seismic Tomography Working Group. Complex lithospheric structure under the central baltic shield from surface wave tomography. *J. Geophys. Res.*, 109:B10303, 2004.

[13] V. Cerveny and I. Psencik. Seis83—numerical modelling of seismicwave fields in 2-d laterally varying structure by the ray method. In E.R. Engdahl, editor, *Documentation of Earthquake algorithms*, number SE-35 in A Solid Earth Geophys., Rep. World Data Cent., 1983.

[14] M. Cherevatova. *Electrical Conductivity Structure of the Lithosphere in Western Fennoscandia from Three-dimensional Magnetotelluric data*. PhD thesis, University of Oulu, 2014.

[15] S. Constable, R. Parker, and C. Constable. Occam's inversion: A practical algorithm for generatlng smooth models from electromagnetic sounding data. *Geophysics*, 53(3):289–300, 1987.

[16] J. S. Daly, V. V. Balagansky, M. J. Timmerman, and M. J. Whitehouse. The lapland-kola orogen: Palaeoproterozoic collision and accretion of the northern fennoscandian lithosphere. In D. G. Gee and R. A. Stephenson, editors, *European Lithosphere Dynamics*, volume 32 of *Geol. Soc. London, Mem. Ser.*, pages 579–598. Geol. Soc. London, 2006.

[17] H. Downes, E. Balaganskaya, A. Beard, R. Liferovich, and D. Demaiffe. Petrogenetic processes in the ultramafic, alkaline and carbonatitic magmatism in the kola alkaline province: A review. *Lithos*, 85:48–75, 2005.

[18] P. Eilu, editor. *Mineral deposits and metallogeny of Fennoscandia*, volume 53. Geological Survey of Finland, 2012.

[19] P. Eilu, P. Sorjonen-Ward, P. Nurmi, and T. Niiranen. A review of gold mineralization styles in finland. *Econ. Geol.*, 95:1329–1353, 2003.

[20] T. Eken, H. Shomali, R. Roberts, and R. Bodvarsson. Upper mantle structure of the baltic shield below the swedish national seismological networks (snsn) resolved by teleseismic tomography. *Geophys. J. Int.*, 169:617–630, 2007.

[21] S. Elo. Interpretations of the gravity anomaly map of finland. *Geophysica*, 33(1):51–80, 1997.

[22] J.R. Evans and U. Achauer. Teleseismic velocity tomography using the ach method: theory and application to continental scale studies. In H.M. Iyer and K. Hirahara, editors, *Seismic Tomography*, pages 319–360. Chapman and Hall, London, 1993.

[23] Gillian R. Foulger, Giuliano F. Panza, Irina M. Artemieva, Ian D. Bastow, Fabio Cammarano, John R. Evans, Warren B. Hamilton, Bruce R. Julian, Michele Lustrino, Hans Thybo, and Tatiana B. Yanovskaya. Caveats on tomographic images. *Terra Nova*, 25:259–281, 2013.

[24] G. Gaál and R. Gorbatschev. An outline of the precambrian evolution of the baltic shield. *Precambrian Research*, 35:15–52, 1987.

[25] R. Gorbatschev and S. Bogdanova. Frontiers in the baltic shield. *Precambrian Res.*, 64:3–21, 1993.

[26] M. Grad and U. Luosto. Seismic models of the crust of the baltic shield along the sveka profile in finland. *Ann. Geophys.*, 5B:639–650, 1987.

[27] M. Grad, T. Tiira, and ESC Working Group. The moho depth map of the european plate. *Geophys. J. Int.*, 176:279–292, 2008.

[28] B. Guggisberg. *Eine zweidimensionale refraktionseismische Interpretation der Geschwindigkeits-Tiefen-Struktur des oberen Erdmantels unter dem Fennoskandischen Schild (Projekt FENNOLORA)*. PhD thesis, ETH, Zürich, 1986.

[29] B. Guggisberg, W. Kaminski, and C. Prodehl. Crustal structure of the fennoscandian shield – a traveltime interpretation of the long-range fennolora seismic refraction profile. *Tectonophysics*, 195:105–137, 1991.

[30] S.-E. Hjelt. *Pregmatic inversion of Geophysical Data*. Springer-Verlag, 1992.

[31] S.-E. Hjelt, T. Korja, E. Kozlovskaya, I. Lahti, J. Yliniemi, and BEAR and SVEKALAPKO Working Groups. Electrical conductivity and seismic velocity structures of the lithosphere beneath the fennoscandian shield. In D.G. Gee and R.A. Stephenson, editors, *European Lithosphere Dynamics*, volume 32 of *Geol. Soc. London, Mem. Ser.* Geol. Soc. London, 2006.

[32] T. Hyvönen, T. Tiira, A. Korja, P. Heikkinen, E. Rautioaho, and SVEKALAPKO Seismic Tomography Working Group. A tomographic crustal velocity model of the central fennoscandian shield. *Geophys. J. Int.*, 168:2010–2026, 2007.

[33] T. Jackson. Survey of mining companies 2014. *Frazer Institute Annual*, 2015.

[34] D.E. James, F.R. Boyd, D. Schutt, D.R. Bell, and R.W. Carlson. Xenolith constraints on seismic velocities in the upper mantle beneath southern africa. *Geochemistry Geophysics Geosystems*, 5:Q01002, 2004.

[35] T. Janik, E. Kozlovskaya, P. Heikkinen, J. Yliniemi, and H. Silvennoinen. Evidence for preservation of crustal root beneath the proterozoic lapland-kola orogen (northern fennoscandian shield) derived from p and s wave velocity models of polar and hukka wide-angle reflection and refraction profiles and fire4 reflection transect. *Journal of Geophysical Research: Solid Earth*, 114(B6):B06308, 2009.

[36] I. Janutyte. *Upper mantle structure around the Trans-European suture zone*. PhD thesis, University of Vilnius, 2014.

[37] J. Kääriäinen and J. Mäkinen. The 1979 – 1996 gravity survey and results of the gravity survey of finland. *Publications of the Finnish Geodetic Institute*, 125:24, 1997.

[38] P.D. Kempton, H. Downes, E.V. Sharkov, V.R. Vetrin, D.A. Ionov, D.A. Carswell, and A. Beard. Petrology and geochemistry of xenoliths from the northern baltic shield: evidence for partial melting and metasomatism in the lower crust beneath an archaean terrane. *Lithos*, 36:157–184, 1995.

[39] B.L. Kennett and E.R. Engdahl. Traveltimes for global earthquake location and phase identification. *Geophys. J. Int.*, 105:429–465, 1991.

[40] R. Kind and L.P. Vinnik. The upper-mantle discontinuities underneath the grf array from p-to-s converted phases. *J. Geophys.*, 62:138–147, 1988.

[41] E. Kissling, J. Ansorge, and A. Baumann. Methodological considerations of 3-d crustal structure modelling by 2-d seismic methods. In P. Heitzmann, L.P.S. Mueller, A. Pfiffner, and A. Steck, editors, *Deep Structure of the Swiss Alps*, pages 31–38. Birkhäuser, 1997.

[42] E. Kissling, S. Husen, and F. Haslinger. Model parameterization in seismic tomography: a choise of consequence for the solution quality. *Phys. Earth Planet. In.*, 123:89–101, 2001.

[43] T. Koistinen, M.B. Stephens, V. Bogatchev, Ø Nordgulen, M. Wennerström, and J. Korhonen. *Geological map of Fennoscandian shield, scale 1:2 000 000.* Geological Surveys of Finland, Norway and Sweden and the North-West Department of Natural Resources of Russia, 2001.

[44] K. Komminaho. Software manual for programs model and xrays—a graphical interface for seis83 program package. *Report No. 20, University of Oulu, Department of Geophysics*, 1998.

[45] J. Korhonen, S. Aaro, T. All, S. Elo, L. Haller, J. Kääriäinen, A. Kulinich, J.R. Skilbrei, D. Solheim, H. Säävuori, R. Vaher, L. Zhdanova, and T. Koistinen. *Bouguer Anomaly Map of the Fennoscandian Shield 1:2 000 000.* Geological Surveys of Finland, Norway and Sweden and Ministry of Natural Resources of Russian Federation, 2002.

[46] A. Korja, T. Korja, U. Luosto, and P. Heikkinen. Seismic and geoelectric evidence for collisional and extensional events in the baltic shield – implications for precambrian crustal evolution. *Tectonophysics*, 219:129–152, 1993.

[47] G.L. Kosarev, N.V. Petersen, L.P. Vinnik, and S.W. Roecker. Receiver function for the tien shan analog broadband network: contrast in the evolution of structure across the talasso-fargana fault. *J. Geophys. Res.*, 98:4437–4448, 1993.

[48] E. Kozlovskaya, S. Elo, S.-E. Hjelt, J. Yliniemi, M. Pirttijärvi, and SVEKALAPKO STWG. 3d density model of the crust of southern and central finland obtained from joint interpretation of svekalapko crustal p-wave velocity model and gravity data. *Geophys. J. Int.*, 158:827–848, 2004.

[49] E. Kozlovskaya, G. Kosarev, I. Aleshin, O. Riznichenko, and I. Sanina. Structure and composition of the crust and upper mantle of the archean-proterozoic boundary in the fennoscandian shield obtained by joint inversion of receiver function and surface wave phase velocity of recording of the svekalapko array. *Geophys. J. Int.*, 175:135–152, 2008.

[50] E. Kozlovskaya and J. Yliniemi. Deep structure of the earth's crust along the sveka profile and its extention to the north-east. *Geophysica*, 1-2:111–123, 1999.

[51] I. Kukkonen, P. Heikkinen, E. Ekdahl, S.-E. Hjelt, J. Yliniemi, E. Jalkanen, and FIRE Working Group. Acquisition and geophysical characteristics of reflection seismic data on fire transects, fennoscandian shield. In I.T. Kukkonen and R. Lahtinen, editors, *Finnish Reflection Experiment FIRE 2001–2005*, volume 43 of *Special Paper*, pages 13–43. Geological Survey of Finland, 2006.

[52] R. Lahtinen, A. A. Garde, and V. A. Melezhik. Paleoproterozoic evolution of fennoscandia and greenland. *Episodes*, 31(1):1–9, 2008.

[53] S. Lebedev, J. Boonen, and J. Trampert. Seismic structure of precambrian lithosphere: New constraints from broad-band surface-wave dispersion. *Lithos*, 109:96–111, 2009.

[54] C.-T. Lee. Compositional variation of density and seismic velocities in natural peridotites at stp conditions: implications for seismic imaging of compositional heterogeneities in the upper mantle. *J. Geophys. Res.*, 108:2441, 2003.

[55] U. Luosto. Structure of the earth's crust in fennoscandia as revealed from refraction and wide-angle reflection studies. *Geophysica*, 33:3–16, 1997.

[56] U. Luosto, E.R. Flueh, Lund C.-E., and POLAR Working group. The crustal structure along the polar profile from seismic refraction investigation. *Tectonophysics*, 162(87-99):51–85, 1989.

[57] U. Luosto and H. Korhonen. Crustal structure of the baltic shield based on off – fennolora refraction data. *Tectonophysics*, 128:183–208, 1986.

[58] U. Luosto, E. Lanne, H. Korhonen, A. Guterch, M. Grad, R. Materzok, and E. Perchuc. Deep structure of the earth's crust on the sveka profile in central finland. *Ann. Geophys.*, 2:559–570, 1984.

[59] E. Luukkonen. Late archean and early proterozoic structural evolution in the kuhmo-suomussalmi terrain, eastern finland. *Ann. Univ. Turkuensis, Ser. A. II*, 78:1–37, 1992.

[60] W. Menke. *Geophysical Data Analysis: Discrete Inverse Theory*, volume 45 of *International Geophysical Series*. Academic Press, London, 1984.

[61] W. D. Mooney, G. Laske, and T. G. Masters. Crust 5.1: A global crustal model at 5° x 5°. *Jour. of Geophys. Res.*, 103(B1):727–747, 1998.

[62] S. Olsson, R. Roberts, and R. Bodvarsson. Moho depth variation in the baltic shield from analysis of converted waves. *GFF*, 130:113–122, 2008.

[63] J. Pak and V. Levin. Receiver functions from multiple-taper spectral correlation estimates. *Bulletin of the Seismological Society of America*, 90(6):1507–1520, 2000.

[64] M.E. Pasyanos and A. Nyblade. A top to bottom lithospheric study of africa and arabia. *Tectonophysics*, 444:27–44, 2007.

[65] N.L. Patison, A. Korja, R. Lahtinen, V.J. Ojala, and FIRE Working Group. Fire seismic reflection profiles 4, 4a and 4b: insights into the crustal structure of northern finland from ranua to näätämö. In I.T. Kukkonen and R. Lahtinen, editors, *Finnish Reflection Experiment FIRE 2001–2005*, volume 43 of *Special Paper*, pages 162–222. Geological Survey of Finland, 2006.

[66] H.A. Pedersen, E. Debayle, V. Maupin, and the POLENET/LAPNET Working Group. Strong lateral variations of lithospheric mantle beneath cratons – example from the baltic shield. *Earth and Plan. Sci. Lett.*, 383:164–172, 2013.

[67] T. Piirainen. The geology of the archean greenstone-granitoid terrain in kuhmo, eastern finland. In E. Marttila, editor, *Archean Geology of the Fennoscandian Shield*, volume 4 of *Special Paper*, pages 39–51. Geological Survey of Finland Special Paper, 1988.

[68] M. Pirttijärvi. Numerical modeling and inversion of geophysical electromagnetic measurements using a thin plate model. *Acta Univ. Ouluensis A*, 403, 2003.

[69] M. Pirttijärvi. *GRABLOX Gravity interpretation and modeling software based on a 3-D block model, version 1.5a User's guide*, 2005.

[70] J. Plomerová and V. Babuška. Long memory of mantle lithosphere fabric – european lab constrained from seismic anisotropy. *Lithos*, 120:131–143, 2010.

[71] J. Plomerová, V. Babuška, L. Vecsey, E. Kozlovskaya, T. Raita, and SSTWG. Proterozoic-archean boundary in the upper mantle of eastern fennoscandia as seen by seismic anisotropy. *J. Geodyn.*, 41:400–410, 2006.

[72] J. Plomerová, L. Vecsey, V. Babuška, and LAPNET Working Group. Domains of archean mantle lithosphere deciphered by seismic anisotrophy – inferences from the lapnet array in northern fennoscandia. *Solid Earth*, 2:303–313, 2011.

[73] W. Pohl. *Economic geology: principles and practice. Metals, minerals, coal and hydrocarbons – introduction to formation and sustainable exploitation of mineral deposits.* Blackwell Publishing Ltd., 2011.

[74] K. Priestley, D. McKenzie, E. Debayle, and S. Pilidou. The african upper mantle and its relationship to tectonics and surface geology. *Geophys. J. Int.*, 175:1105–1126, 2008.

[75] S. Sandoval, E. Kissling, J. Ansorge, and SVEKALAPKO STWG. High-resolution body wave tomography beneath the svekalapko array: Ii. anomalous upper mantle structure beneath the central baltic shield. *Geophys. J. Int.*, 157:200–214, 2004.

[76] D. Schutt and C. Lesher. The effects of melt depletion on the density and seismic velocity of garnet and spinel lherzolite. *Jour. of Geophys. Res.*, 111:B05401, 2006.

[77] P.M. Shearer. *Introduction to Seismology.* Cambridge University Press, 1999.

[78] Z.H. Shomali, R.G. Roberts, L.B. Pedersen, and TOR Working Group. Lithospheric structure of the tornquist zone resolved by nonlinear p and s teleseismic tomography along the tor array. *Tectonophysics*, 416:133–149, 2006.

[79] M. Spada, I. Bianchi, E. Kissling, R. Di Stefano, N. Piana Agostinetti, and S. Wiemer. Combining controlled-source seismology and receiver function information to derive reference 3-d moho topography for italy. *Geophys. J. Int.*, 194(2):1050–1068, 2013.

[80] L. K. Steck and W.A. Prothero. A 3-d ray-tracer for teleseismic body-wave arrival-times. *B. Seismol. Soc. Am.*, 81:1332–1339, 1991.

[81] K. Taipale. The geology and geochemistry of the archean kuhmo greenstone-granite terrain in the tipasjÂ¨arvi area, eastern finland. *Acta Univ. Ouluensis A*, 151(98, Geol 5), 1983.

[82] K. Taipale. Volcanism in the archean kuhmo greenstone belt, eastern finland. In E. Marttila, editor, *Archean Geology of the Fennoscandian Shield*, volume 4, pages 151–176. Geological Survey of Finland, 1988.

[83] M. Tesauro, M. Kaban, and S. Cloetingh. Eucrust-07: a new reference model for the european crust. *Geoph. Res. Lett.*, 35(5):L05313, 2008.

[84] T. Tiira, T. Janik, E. Kozlovskaya, M. Grad, A. Korja, K. Komminaho, E. Hegedüs, C. Attila Kovács, H. Silvennoinen, and E. Bru ückl. Crustal architecture of the inverted central lapland rift along the hukka 2007 profile. *Pure and Appl. Geophys.*, 171(7):1129–1152, 2014.

[85] M. Villemaire, F.A. Darbyshire, and I.D. Bastow. Evolution of the mantle from archean to phanerozoic and its modification during subsequent hotspot tectonism : seismic evidence from eastern north america. *Jour. of Geophys. Res.*, 117:B12302, 2012.

[86] L. Vinnik, S. Oreshin, E. Kozlovskaya, G. Kosarev, K. Piiponen, and H. Silvennoinen. Lithosphere and asthenosphere under central fennoscandia from p- and s-wave receiver functions. *Earth and Plan. Sci. Lett.*, submitted.

[87] L. Vinnik, Oreshin S., L. Makeyeva, D. Peregoudov, E. Kozlovskaya, and POLENET/LAPNET Working Group. Anisotropic lithosphere under the fennoscandian shield from p receiver functions and sks waveforms of the polenet/lapnet array. *Tectonophysics*, 628:45–54, 2014.

[88] L.P. Vinnik. Detection of waves converted from p to sv in the mantle. *Phys. Earth Planet Inter.*, 15:39–45, 1977.

[89] F. Waldhauser, E. Kissling, J. Ansorge, and St. Mueller. Three-dimensional interface modeling with two-dimensional seismic data: the alpine crust–mantle boundary. *Geophys. J. Int.*, 135:264–278, 1998.

[90] P. Weihed, N. Arndt, C. Billström, J. C. Duchesne, P. Eilu, O. Martinsson, H. Papunen, and Lahtinen R. Precambrian geodynamics and ore formation: the fennoscandian shield. *Ore Geol. Rew.*, 27:273–322, 2005.

[91] C.M. Weiland, L.K. Steck, P.B. Dawson, and V.A. Korneev. Nonlinear teleseismic tomography at long valley caldera, using three-dimensional minimum travel time ray tracing. *J. Geophys. Res.*, 100:20379–20390, 1995.

[92] J. Woodard. *Genesis and Emplacement of Carbonatites and Lamprophyres in the Svecofennian Domain*. PhD thesis, University of Turku, 2010.

[93] H. Yuan and V. Levin. Stratified seismic anisotropy and the lithosphere-asthenosphere boundary beneath eastern north america. *J. Geophys. Res.*, 119:3096–3114, 2014.

[94] C.A. Zelt. *ZPLOT—An Interactive Plotting and Picking Program for Seismic Data*. Bullard Lab, University of Cambridge, UK, 1994.

ISBN 978-952-62-1067-4 (paperback)
ISBN 978-952-62-1068-1 (pdf)
ISSN 1456-3673